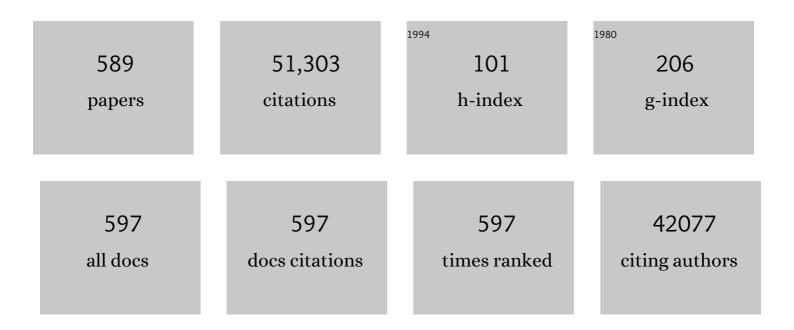
List of Publications by Year in descending order

Source: https://exaly.com/author-pdf/507106/publications.pdf Version: 2024-02-01



#	Article	IF	CITATIONS
1	Epitaxial BiFeO3 Multiferroic Thin Film Heterostructures. Science, 2003, 299, 1719-1722.	12.6	5,548
2	Pseudocapacitive Contributions to Electrochemical Energy Storage in TiO ₂ (Anatase) Nanoparticles. Journal of Physical Chemistry C, 2007, 111, 14925-14931.	3.1	3,863
3	Ordered mesoporous α-MoO3 with iso-oriented nanocrystalline walls for thin-film pseudocapacitors. Nature Materials, 2010, 9, 146-151.	27.5	2,801
4	Multiferroic BaTiO3-CoFe2O4 Nanostructures. Science, 2004, 303, 661-663.	12.6	2,051
5	Rational Design of Metalâ€Organic Framework Derived Hollow NiCo ₂ O ₄ Arrays for Flexible Supercapacitor and Electrocatalysis. Advanced Energy Materials, 2017, 7, 1602391.	19.5	874
6	Two dimensional hexagonal boron nitride (2D-hBN): synthesis, properties and applications. Journal of Materials Chemistry C, 2017, 5, 11992-12022.	5.5	732
7	Graphene-based materials for supercapacitor electrodes – A review. Journal of Materiomics, 2016, 2, 37-54.	5.7	620
8	Hollow Mo-doped CoP nanoarrays for efficient overall water splitting. Nano Energy, 2018, 48, 73-80.	16.0	608
9	A Highâ€Rate and Stable Quasiâ€Solidâ€State Zincâ€Ion Battery with Novel 2D Layered Zinc Orthovanadate Array. Advanced Materials, 2018, 30, e1803181.	21.0	571
10	Intrinsically fluorescent carbon dots with tunable emission derived from hydrothermal treatment of glucose in the presence of monopotassium phosphate. Chemical Communications, 2011, 47, 11615.	4.1	529
11	Hafnia and hafnia-toughened ceramics. Journal of Materials Science, 1992, 27, 5397-5430.	3.7	511
12	A Flexible Quasiâ€Solidâ€State Nickel–Zinc Battery with High Energy and Power Densities Based on 3D Electrode Design. Advanced Materials, 2016, 28, 8732-8739.	21.0	479
13	Multiferroic bismuth ferrite-based materials for multifunctional applications: Ceramic bulks, thin films and nanostructures. Progress in Materials Science, 2016, 84, 335-402.	32.8	478
14	Iron Oxide-Decorated Carbon for Supercapacitor Anodes with Ultrahigh Energy Density and Outstanding Cycling Stability. ACS Nano, 2015, 9, 5198-5207.	14.6	441
15	Hollow Co ₃ O ₄ Nanosphere Embedded in Carbon Arrays for Stable and Flexible Solid‧tate Zinc–Air Batteries. Advanced Materials, 2017, 29, 1704117.	21.0	407
16	In Situ Grown Epitaxial Heterojunction Exhibits Highâ€Performance Electrocatalytic Water Splitting. Advanced Materials, 2018, 30, e1705516.	21.0	375
17	Zirconia-toughened alumina (ZTA) ceramics. Journal of Materials Science, 1989, 24, 3421-3440.	3.7	372
18	Single Co Atoms Anchored in Porous N-Doped Carbon for Efficient Zincâ^'Air Battery Cathodes. ACS Catalysis, 2018, 8, 8961-8969.	11.2	364

#	Article	IF	CITATIONS
19	Metal Phosphides and Phosphatesâ€based Electrodes for Electrochemical Supercapacitors. Small, 2017, 13, 1701530.	10.0	318
20	Ferroelectricity of CH ₃ NH ₃ PbI ₃ Perovskite. Journal of Physical Chemistry Letters, 2015, 6, 1155-1161.	4.6	295
21	Copper Single Atoms Anchored in Porous Nitrogen-Doped Carbon as Efficient pH-Universal Catalysts for the Nitrogen Reduction Reaction. ACS Catalysis, 2019, 9, 10166-10173.	11.2	284
22	Cactusâ€Like NiCoP/NiCoâ€OH 3D Architecture with Tunable Composition for Highâ€Performance Electrochemical Capacitors. Advanced Functional Materials, 2018, 28, 1800036.	14.9	274
23	Sulfur-doped cobalt phosphide nanotube arrays for highly stable hybrid supercapacitor. Nano Energy, 2017, 39, 162-171.	16.0	273
24	Highâ€Performance Flexible Solidâ€State Ni/Fe Battery Consisting of Metal Oxides Coated Carbon Cloth/Carbon Nanofiber Electrodes. Advanced Energy Materials, 2016, 6, 1601034.	19.5	262
25	The growth of nickel-manganese and cobalt-manganese layered double hydroxides on reduced graphene oxide for supercapacitor. Electrochimica Acta, 2016, 206, 108-115.	5.2	259
26	Effects of grain size on the dielectric properties and tunabilities of sol–gel derived Ba(Zr0.2Ti0.8)O3 ceramics. Solid State Communications, 2004, 131, 163-168.	1.9	252
27	Epitaxial BiFeO3 thin films on Si. Applied Physics Letters, 2004, 85, 2574-2576.	3.3	249
28	Metal–organic framework derived hollow CoS ₂ nanotube arrays: an efficient bifunctional electrocatalyst for overall water splitting. Nanoscale Horizons, 2017, 2, 342-348.	8.0	247
29	Decorating Co/CoNx nanoparticles in nitrogen-doped carbon nanoarrays for flexible and rechargeable zinc-air batteries. Energy Storage Materials, 2019, 16, 243-250.	18.0	244
30	MOF-derived nanohybrids for electrocatalysis and energy storage: current status and perspectives. Chemical Communications, 2018, 54, 5268-5288.	4.1	237
31	Perovskites for photovoltaics: a combined review of organic–inorganic halide perovskites and ferroelectric oxide perovskites. Journal of Materials Chemistry A, 2015, 3, 18809-18828.	10.3	232
32	TMD-based highly efficient electrocatalysts developed by combined computational and experimental approaches. Chemical Society Reviews, 2018, 47, 4332-4356.	38.1	232
33	Oxygen-vacancy-related relaxation and scaling behaviors of <mml:math xmlns:mml="http://www.w3.org/1998/Math/MathML" display="inline"><mml:mrow><mml:msub><mml:mrow><mml:mtext>Bi</mml:mtext></mml:mrow><mml:mrow> Physical Review B. 2010. 82</mml:mrow></mml:msub></mml:mrow></mml:math 	< <mark>3:2</mark> <mml:mn< td=""><td>>0.9</td></mml:mn<>	> 0. 9
34	Significant Role of Al in Ternary Layered Double Hydroxides for Enhancing Electrochemical Performance of Flexible Asymmetric Supercapacitor. Advanced Functional Materials, 2019, 29, 1903879.	14.9	228
35	Cobalt oxide and N-doped carbon nanosheets derived from a single two-dimensional metal–organic framework precursor and their application in flexible asymmetric supercapacitors. Nanoscale Horizons, 2017, 2, 99-105.	8.0	227
36	Mechanochemical synthesis of nanocrystalline hydroxyapatite from CaO and CaHPO4. Biomaterials, 2001, 22, 2705-2712.	11.4	217

#	Article	IF	CITATIONS
37	Oneâ€dimensional and twoâ€dimensional synergized nanostructures for highâ€performing energy storage and conversion. InformaÄnÃ-Materiály, 2020, 2, 3-32.	17.3	206
38	Silica-based nanocapsules: synthesis, structure control and biomedical applications. Chemical Society Reviews, 2015, 44, 315-335.	38.1	205
39	Rational Design of Holey 2D Nonlayered Transition Metal Carbide/Nitride Heterostructure Nanosheets for Highly Efficient Water Oxidation. Advanced Energy Materials, 2019, 9, 1803768.	19.5	204
40	Surfaceâ€Chargeâ€Mediated Formation of Hâ€īiO ₂ @Ni(OH) ₂ Heterostructures for Highâ€Performance Supercapacitors. Advanced Materials, 2017, 29, 1604164.	21.0	203
41	(Ni,Co)Se ₂ /NiCoâ€LDH Core/Shell Structural Electrode with the Cactusâ€Like (Ni,Co)Se ₂ Core for Asymmetric Supercapacitors. Small, 2019, 15, e1803895.	10.0	203
42	Hierarchical Microâ€Nano Sheet Arrays of Nickel–Cobalt Double Hydroxides for Highâ€Rate Ni–Zn Batteries. Advanced Science, 2019, 6, 1802002.	11.2	202
43	CuO nanowires synthesized by thermal oxidation route. Journal of Alloys and Compounds, 2008, 454, 268-273.	5.5	200
44	Controllable MnCo ₂ S ₄ nanostructures for high performance hybrid supercapacitors. Journal of Materials Chemistry A, 2017, 5, 7494-7506.	10.3	198
45	Efficient Hydrogen Evolution of Oxidized Niâ€N ₃ Defective Sites for Alkaline Freshwater and Seawater Electrolysis. Advanced Materials, 2021, 33, e2003846.	21.0	198
46	Composition and poling condition-induced electrical behavior of (Ba0.85Ca0.15)(Ti1â^'xZrx)O3 lead-free piezoelectric ceramics. Journal of the European Ceramic Society, 2012, 32, 891-898.	5.7	197
47	3Dâ€Printed MOFâ€Derived Hierarchically Porous Frameworks for Practical Highâ€Energy Density Li–O ₂ Batteries. Advanced Functional Materials, 2019, 29, 1806658.	14.9	197
48	All‣olid‣tate Fiber Supercapacitors with Ultrahigh Volumetric Energy Density and Outstanding Flexibility. Advanced Energy Materials, 2019, 9, 1802753.	19.5	197
49	Synthesis of Fe3O4 nanoparticles from emulsions. Journal of Materials Chemistry, 2001, 11, 1704-1709.	6.7	193
50	Integrated Hierarchical Carbon Flake Arrays with Hollow Pâ€Doped CoSe ₂ Nanoclusters as an Advanced Bifunctional Catalyst for Zn–Air Batteries. Advanced Functional Materials, 2018, 28, 1804846.	14.9	192
51	Synergizing Mo Single Atoms and Mo ₂ C Nanoparticles on CNTs Synchronizes Selectivity and Activity of Electrocatalytic N ₂ Reduction to Ammonia. Advanced Materials, 2020, 32, e2002177.	21.0	190
52	Stitching of Zn ₃ (OH) ₂ V ₂ O ₇ ·2H ₂ O 2D Nanosheets by 1D Carbon Nanotubes Boosts Ultrahigh Rate for Wearable Quasi-Solid-State Zinc-Ion Batteries. ACS Nano, 2020, 14, 842-853.	14.6	183
53	Ni-Doped Cobalt–Cobalt Nitride Heterostructure Arrays for High-Power Supercapacitors. ACS Energy Letters, 2018, 3, 2462-2469.	17.4	182
54	Ceramic-based membranes for water and wastewater treatment. Colloids and Surfaces A: Physicochemical and Engineering Aspects, 2019, 578, 123513.	4.7	179

#	Article	IF	CITATIONS
55	Bimetallic Nickel Cobalt Sulfide as Efficient Electrocatalyst for Zn–Air Battery and Water Splitting. Nano-Micro Letters, 2019, 11, 2.	27.0	179
56	Generation and Dynamics of an Endogenous, Self-Generated Signaling Gradient across a Migrating Tissue. Cell, 2013, 155, 674-687.	28.9	174
57	Potential-Dependent Phase Transition and Mo-Enriched Surface Reconstruction of γ-CoOOH in a Heterostructured Co-Mo ₂ C Precatalyst Enable Water Oxidation. ACS Catalysis, 2020, 10, 4411-4419.	11.2	174
58	Improving the magnetic properties of hydrothermally synthesized barium ferrite. Journal of Magnetism and Magnetic Materials, 1999, 195, 452-459.	2.3	172
59	NiFe2O4 ultrafine particles prepared by co-precipitation/mechanical alloying. Journal of Magnetism and Magnetic Materials, 1999, 205, 249-254.	2.3	170
60	Role of room-temperature phase transition in the electrical properties of (Ba, Ca)(Ti, Zr)O3 ceramics. Scripta Materialia, 2011, 65, 771-774.	5.2	170
61	NiFe2O4 nanoparticles formed in situ in silica matrix by mechanical activation. Journal of Applied Physics, 2002, 91, 6015-6020.	2.5	165
62	Fabrication of (NH4)2V3O8 nanoparticles encapsulated in amorphous carbon for high capacity electrodes in aqueous zinc ion batteries. Chemical Engineering Journal, 2020, 382, 122844.	12.7	164
63	Ferroelectric HfO ₂ -based materials for next-generation ferroelectric memories. Journal of Advanced Dielectrics, 2016, 06, 1630003.	2.4	163
64	Manipulating unidirectional fluid transportation to drive sustainable solar water extraction and brine-drenching induced energy generation. Energy and Environmental Science, 2020, 13, 4891-4902.	30.8	162
65	Heterojunction engineering of MoSe2/MoS2 with electronic modulation towards synergetic hydrogen evolution reaction and supercapacitance performance. Chemical Engineering Journal, 2019, 359, 1419-1426.	12.7	160
66	Intrinsically fluorescent nitrogen-containing carbon nanoparticles synthesized by a hydrothermal process. Carbon, 2011, 49, 5207-5212.	10.3	156
67	Selfâ€Powered Waterâ€Splitting Devices by Core–Shell NiFe@Nâ€Graphiteâ€Based Zn–Air Batteries. Advanc Functional Materials, 2018, 28, 1706928.	ed 14.9	155
68	Mechanochemical Synthesis of Lead Zirconate Titanate from Mixed Oxides. Journal of the American Ceramic Society, 1999, 82, 1687-1692.	3.8	154
69	Nanoframes of Co ₃ O ₄ –Mo ₂ N Heterointerfaces Enable Highâ€Performance Bifunctionality toward Both Electrocatalytic HER and OER. Advanced Functional Materials, 2022, 32, 2107382.	14.9	153
70	Synthesis and piezoresponse of highly ordered Pb(Zr0.53Ti0.47)O3 nanowire arrays. Applied Physics Letters, 2004, 85, 4190-4192.	3.3	151
71	Processing of hydroxyapatite via microemulsion and emulsion routes. Biomaterials, 1997, 18, 1433-1439.	11.4	146
72	Flexible Asymmetric Supercapacitor Based on Structureâ€Optimized Mn ₃ O ₄ /Reduced Graphene Oxide Nanohybrid Paper with High Energy and Power Density. Advanced Functional Materials, 2015, 25, 7291-7299.	14.9	146

#	Article	IF	CITATIONS
73	An ultrafine barium ferrite powder of high coercivity from water-in-oil microemulsion. Journal of Magnetism and Magnetic Materials, 1998, 184, 344-354.	2.3	145
74	Transparent nanohybrids of nanocrystalline TiO2 in PMMA with unique nonlinear optical behavior. Journal of Materials Chemistry, 2003, 13, 1475.	6.7	144
75	Controlling the crystallinity and nonlinear optical properties of transparent TiO2–PMMA nanohybrids. Journal of Materials Chemistry, 2004, 14, 2978-2987.	6.7	144
76	Ferroelectric and Impedance Behavior of La―and Tiâ€Codoped BiFeO ₃ Thin Films. Journal of the American Ceramic Society, 2010, 93, 2795-2803.	3.8	142
77	BiFeO3 thin films of (1 1 1)-orientation deposited on SrRuO3 buffered Pt/TiO2/SiO2/Si(1 0 0) substrates. Acta Materialia, 2010, 58, 1688-1697.	7.9	141
78	Impedance study of giant dielectric permittivity in BaFe0.5Nb0.5O3 perovskite ceramic. Current Applied Physics, 2010, 10, 21-25.	2.4	141
79	Zn ²⁺ Preâ€Intercalation Stabilizes the Tunnel Structure of MnO ₂ Nanowires and Enables Zincâ€Ion Hybrid Supercapacitor of Batteryâ€Level Energy Density. Small, 2020, 16, e2000091.	10.0	139
80	Design and Manufacture of 3D-Printed Batteries. Joule, 2021, 5, 89-114.	24.0	137
81	Synthesis of PEOlated Fe ₃ O ₄ @SiO ₂ Nanoparticles via Bioinspired Silification for Magnetic Resonance Imaging. Advanced Functional Materials, 2010, 20, 722-731.	14.9	132
82	Electrocatalytic reduction of oxygen by a platinum nanoparticle/carbon nanotube composite electrode. Journal of Electroanalytical Chemistry, 2005, 577, 295-302.	3.8	130
83	Effects of nitrogen doping on supercapacitor performance of a mesoporous carbon electrode produced by a hydrothermal soft-templating process. Journal of Materials Chemistry A, 2014, 2, 11753.	10.3	127
84	Ferroelectric and electrical behavior of (Na0.5Bi0.5)TiO3 thin films. Applied Physics Letters, 2004, 85, 804-806.	3.3	126
85	Synergizing in-grown Ni3N/Ni heterostructured core and ultrathin Ni3N surface shell enables self-adaptive surface reconfiguration and efficient oxygen evolution reaction. Nano Energy, 2020, 78, 105355.	16.0	126
86	Freestanding Metal–Organic Frameworks and Their Derivatives: An Emerging Platform for Electrochemical Energy Storage and Conversion. Chemical Reviews, 2022, 122, 10087-10125.	47.7	126
87	CuCo ₂ S ₄ Nanosheets@Nâ€Doped Carbon Nanofibers by Sulfurization at Room Temperature as Bifunctional Electrocatalysts in Flexible Quasiâ€Solidâ€State Zn–Air Batteries. Advanced Science, 2019, 6, 1900628.	11.2	123
88	Aqueous Rechargeable Multivalent Metalâ€ion Batteries: Advances and Challenges. Advanced Energy Materials, 2021, 11, 2100608.	19.5	122
89	Conformal dispersed cobalt nanoparticles in hollow carbon nanotube arrays for flexible Zn-air and Al-air batteries. Chemical Engineering Journal, 2019, 369, 988-995.	12.7	121
90	Porous NiCo2S4/FeOOH nanowire arrays with rich sulfide/hydroxide interfaces enable high OER activity. Nano Energy, 2020, 78, 105230.	16.0	121

#	Article	IF	CITATIONS
91	In situ coupled amorphous cobalt nitride with nitrogen-doped graphene aerogel as a trifunctional electrocatalyst towards Zn-air battery deriven full water splitting. Applied Catalysis B: Environmental, 2019, 259, 118100.	20.2	120
92	An improvement in processing of hydroxyapatite ceramics. Journal of Materials Science, 1995, 30, 3061-3074.	3.7	117
93	2D carbide nanomeshes and their assembling into 3D microflowers for efficient water splitting. Applied Catalysis B: Environmental, 2019, 243, 678-685.	20.2	116
94	Nurturing the marriages of single atoms with atomic clusters and nanoparticles for better heter heter heterogeneous electrocatalysis. , 2022, 1, 51-87.		114
95	Heterogeneous Single Atom Electrocatalysis, Where "Singles―Are "Married― Advanced Energy Materials, 2020, 10, 1903181.	19.5	113
96	Gold-Cluster Sensors Formed Electrochemically at Boron-Doped-Diamond Electrodes: Detection of Dopamine in the Presence of Ascorbic Acid and Thiols. Advanced Functional Materials, 2005, 15, 639-647.	14.9	110
97	Activation of the MoSe ₂ basal plane and Se-edge by B doping for enhanced hydrogen evolution. Journal of Materials Chemistry A, 2018, 6, 510-515.	10.3	110
98	Ultrafast optical nonlinearity in poly(methylmethacrylate)-TiO2 nanocomposites. Applied Physics Letters, 2003, 82, 2691-2693.	3.3	109
99	Control of Synaptic Plasticity Learning of Ferroelectric Tunnel Memristor by Nanoscale Interface Engineering. ACS Applied Materials & Interfaces, 2018, 10, 12862-12869.	8.0	109
100	Effect of dwell time during sintering on piezoelectric properties of (Ba0.85Ca0.15)(Ti0.90Zr0.10)O3 lead-free ceramics. Journal of Alloys and Compounds, 2011, 509, L359-L361.	5.5	107
101	Ferromagnetic, ferroelectric, and fatigue behavior of (111)-oriented BiFeO3/(Bi1/2Na1/2)TiO3 lead-free bilayered thin films. Applied Physics Letters, 2009, 94, .	3.3	106
102	3D-printed electrodes for lithium metal batteries with high areal capacity and high-rate capability. Energy Storage Materials, 2020, 24, 336-342.	18.0	105
103	Hollow Carbon Nanoparticles of Tunable Size and Wall Thickness by Hydrothermal Treatment of α-Cyclodextrin Templated by F127 Block Copolymers. Chemistry of Materials, 2013, 25, 704-710.	6.7	103
104	Conformally deposited NiO on a hierarchical carbon support for high-power and durable asymmetric supercapacitors. Journal of Materials Chemistry A, 2015, 3, 23283-23288.	10.3	103
105	Bifunctional Oxygen Electrocatalyst of Mesoporous Ni/NiO Nanosheets for Flexible Rechargeable Zn–Air Batteries. Nano-Micro Letters, 2020, 12, 68.	27.0	103
106	Three Dimensionally Free-Formable Graphene Foam with Designed Structures for Energy and Environmental Applications. ACS Nano, 2020, 14, 937-947.	14.6	101
107	All-in-one stretchable coaxial-fiber strain sensor integrated with high-performing supercapacitor. Energy Storage Materials, 2020, 25, 124-130.	18.0	100
108	Synthesizing Nanocrystalline Pb(Zn1/3Nb2/3)O3 Powders from Mixed Oxides. Journal of the American Ceramic Society, 1999, 82, 477-479.	3.8	98

#	Article	IF	CITATIONS
109	Formation of Nanocrystalline Hydroxyapatite in Nonionic Surfactant Emulsions. Langmuir, 1999, 15, 7472-7477.	3.5	97
110	Processing of fine hydroxyapatite powders via an inverse microemulsion route. Materials Letters, 1996, 28, 431-436.	2.6	96
111	Mutual Ferromagnetic–Ferroelectric Coupling in Multiferroic Copperâ€Đoped ZnO. Advanced Materials, 2011, 23, 1635-1640.	21.0	96
112	Hybrid Fe ₂ O ₃ Nanoparticle Clusters/rGO Paper as an Effective Negative Electrode for Flexible Supercapacitors. Chemistry of Materials, 2016, 28, 7296-7303.	6.7	95
113	Surface nitridation of nickel-cobalt alloy nanocactoids raises the performance of water oxidation and splitting. Applied Catalysis B: Environmental, 2020, 270, 118889.	20.2	95
114	Orientation dependence of ferroelectric behavior of BiFeO3 thin films. Journal of Applied Physics, 2009, 106, .	2.5	94
115	Manganeseâ€Oxideâ€Based Electrode Materials for Energy Storage Applications: How Close Are We to the Theoretical Capacitance?. Advanced Materials, 2018, 30, e1802569.	21.0	94
116	Recent Progress in Twoâ€Dimensional Layered Double Hydroxides and Their Derivatives for Supercapacitors. ChemSusChem, 2020, 13, 1226-1254.	6.8	94
117	Engineering the Coordination Environment of Single Cobalt Atoms for Efficient Oxygen Reduction and Hydrogen Evolution Reactions. ACS Catalysis, 2021, 11, 4498-4509.	11.2	94
118	Recent Development of Advanced Electrode Materials by Atomic Layer Deposition for Electrochemical Energy Storage. Advanced Science, 2016, 3, 1500405.	11.2	93
119	Cage-confinement pyrolysis route to size-controlled molybdenum-based oxygen electrode catalysts: From isolated atoms to clusters and nanoparticles. Nano Energy, 2020, 67, 104288.	16.0	93
120	Enhanced Photocatalysis by Doping Cerium into Mesoporous Titania Thin Films. Journal of Physical Chemistry C, 2009, 113, 21406-21412.	3.1	92
121	Ferroelectric Transistors with Nanowire Channel: Toward Nonvolatile Memory Applications. ACS Nano, 2009, 3, 700-706.	14.6	89
122	Electrical and magnetic properties of multiferroic BiFeO3/CoFe2O4 heterostructure. Journal of Applied Physics, 2008, 104, .	2.5	88
123	Photovoltaic effect in an indium-tin-oxide/ZnO/BiFeO3/Pt heterostructure. Applied Physics Letters, 2014, 105, .	3.3	85
124	Enlarged Interlayer Spacing in Cobalt–Manganese Layered Double Hydroxide Guiding Transformation to Layered Structure for High Supercapacitance. ACS Applied Materials & Interfaces, 2019, 11, 23236-23243.	8.0	85
125	Z-scheme carbon-bridged Bi2O3/TiO2 nanotube arrays to boost photoelectrochemical detection performance. Applied Catalysis B: Environmental, 2019, 248, 255-263.	20.2	85
126	Atomic layer deposition of Co ₃ O ₄ on carbon nanotubes/carbon cloth for high-capacitance and ultrastable supercapacitor electrode. Nanotechnology, 2015, 26, 094001.	2.6	84

#	Article	IF	CITATIONS
127	3D Graphene-Nickel Hydroxide Hydrogel Electrode for High-Performance Supercapacitor. Electrochimica Acta, 2016, 196, 653-660.	5.2	83
128	Ultrafine Molybdenum Carbide Nanocrystals Confined in Carbon Foams via a Colloid onfinement Route for Efficient Hydrogen Production. Small Methods, 2018, 2, 1700396.	8.6	83
129	Mechanically Activating Nucleation and Growth of Complex Perovskites. Journal of Solid State Chemistry, 2000, 154, 321-328.	2.9	81
130	Sintering temperature-induced electrical properties of (Ba0.90Ca0.10)(Ti0.85Zr0.15)O3 lead-free ceramics. Materials Research Bulletin, 2012, 47, 1281-1284.	5.2	81
131	Direct observation of room-temperature out-of-plane ferroelectricity and tunneling electroresistance at the two-dimensional limit. Nature Communications, 2018, 9, 3319.	12.8	81
132	NH ₄ V ₃ O ₈ ·0.5H ₂ O nanobelts with intercalated water molecules as a high performance zinc ion battery cathode. Materials Chemistry Frontiers, 2020, 4, 1434-1443.	5.9	81
133	Effects of mechanical activation on the sintering and dielectric properties of oxide-derived PZT. Acta Materialia, 1999, 47, 2633-2639.	7.9	80
134	Multiferroic behavior and impedance spectroscopy of bilayered BiFeO3/CoFe2O4 thin films. Journal of Applied Physics, 2009, 105, .	2.5	80
135	2D Metal–Organic Frameworks Derived Nanocarbon Arrays for Substrate Enhancement in Flexible Supercapacitors. Small, 2018, 14, e1702641.	10.0	80
136	3D-Printing of Pure Metal–Organic Framework Monoliths. , 2019, 1, 147-153.		80
137	Strain stabilized nickel hydroxide nanoribbons for efficient water splitting. Energy and Environmental Science, 2020, 13, 229-237.	30.8	78
138	Binder-free 3D printing of covalent organic framework (COF) monoliths for CO2 adsorption. Chemical Engineering Journal, 2021, 403, 126333.	12.7	78
139	Size effect on the ferroelectric phase transition in SrBi2Ta2O9 nanoparticles. Journal of Applied Physics, 2003, 94, 618-620.	2.5	77
140	3D Nanostructure of Carbon Nanotubes Decorated Co 3 O 4 Nanowire Arrays for High Performance Supercapacitor Electrode. Electrochimica Acta, 2015, 163, 9-15.	5.2	77
141	Nanosized hydroxyapatite powders from microemulsions and emulsions stabilized by a biodegradable surfactant. Journal of Materials Chemistry, 1999, 9, 1635-1639.	6.7	75
142	Metal–organic framework-derived integrated nanoarrays for overall water splitting. Journal of Materials Chemistry A, 2018, 6, 9009-9018.	10.3	74
143	Hollow spheres of nanocarbon and their manganese dioxide hybrids derived fromÂsoft template for supercapacitor application. Journal of Power Sources, 2013, 240, 713-720.	7.8	73
144	Activation of sucrose-derived carbon spheres for high-performance supercapacitor electrodes. RSC Advances, 2015, 5, 9307-9313.	3.6	73

#	Article	IF	CITATIONS
145	Transition-metal-doped NiSe2 nanosheets towards efficient hydrogen evolution reactions. Nano Research, 2018, 11, 6051-6061.	10.4	72
146	Nanoflakes of Ni–Co LDH and Bi ₂ O ₃ Assembled in 3D Carbon Fiber Network for High-Performance Aqueous Rechargeable Ni/Bi Battery. ACS Applied Materials & Interfaces, 2017, 9, 26008-26015.	8.0	71
147	Leakage mechanism of cation -modified BiFeO3 thin film. AIP Advances, 2011, 1, .	1.3	70
148	Black Phosphorus@Ti ₃ C ₂ T _{<i>x</i>} MXene Composites with Engineered Chemical Bonds for Commercial-Level Capacitive Energy Storage. ACS Nano, 2021, 15, 12975-12987.	14.6	70
149	Substrate-Assisted Crystallization and Photocatalytic Properties of Mesoporous TiO2 Thin Films. Chemistry of Materials, 2006, 18, 2917-2923.	6.7	69
150	Surfactant-modified chemically reduced graphene oxide for electrochemical supercapacitors. RSC Advances, 2014, 4, 26398-26406.	3.6	69
151	Diblock Copolymer Templated Nanohybrid Thin Films of Highly Ordered TiO2Nanoparticle Arrays in PMMA Matrix. Chemistry of Materials, 2006, 18, 5876-5889.	6.7	68
152	3D TiO2@Ni(OH)2 Core-shell Arrays with Tunable Nanostructure for Hybrid Supercapacitor Application. Scientific Reports, 2015, 5, 13940.	3.3	68
153	Ferroelectric domains and piezoelectricity in monocrystalline Pb(Zr,Ti)O3 nanowires. Applied Physics Letters, 2007, 90, 133107.	3.3	67
154	Flexible supercapacitor of high areal performance with vanadium/cobalt oxides on carbon nanofibers as a binder-free membrane electrode. Chemical Engineering Journal, 2020, 402, 126294.	12.7	67
155	Unravelling V ₆ O ₁₃ Diffusion Pathways <i>via</i> CO ₂ Modification for High-Performance Zinc Ion Battery Cathode. ACS Nano, 2021, 15, 1273-1281.	14.6	67
156	Multiferroic BiFeO3 thin films deposited on SrRuO3 buffer layer by rf sputtering. Journal of Applied Physics, 2007, 101, 054104.	2.5	66
157	Photoluminescence and Raman scattering studies on PbTiO3 nanowires fabricated by hydrothermal method at low temperature. Applied Physics Letters, 2006, 88, 193120.	3.3	65
158	Effects of SrRuO3 buffer layer thickness on multiferroic (Bi0.90La0.10)(Fe0.95Mn0.05)O3 thin films. Journal of Applied Physics, 2009, 106, .	2.5	65
159	Stretchable fiber-shaped lithium metal anode. Energy Storage Materials, 2019, 22, 179-184.	18.0	65
160	Ultrafine ferrite particles prepared by coprecipitation/mechanical milling. Materials Letters, 2000, 44, 19-22.	2.6	64
161	Migration Kinetics of Oxygen Vacancies in Mn-Modified BiFeO ₃ Thin Films. ACS Applied Materials & amp; Interfaces, 2011, 3, 2504-2511.	8.0	64
162	Synthesis of monodispersed SnO2@C composite hollow spheres for lithium ion battery anode applications. Journal of Materials Chemistry, 2011, 21, 17448.	6.7	64

#	Article	IF	CITATIONS
163	Lithiophilic polymer interphase anchored on laser-punched 3D holey Cu matrix enables uniform lithium nucleation leading to super-stable lithium metal anodes. Energy Storage Materials, 2020, 29, 84-91.	18.0	64
164	PEOlated Micelle/Silica as Dual-Layer Protection of Quantum Dots for Stable and Targeted Bioimaging. Chemistry of Materials, 2013, 25, 2976-2985.	6.7	63
165	Key issues facing electrospun carbon nanofibers in energy applications: on-going approaches and challenges. Nanoscale, 2020, 12, 13225-13248.	5.6	63
166	Giant strain in PbZr0.2Ti0.8O3 nanowires. Applied Physics Letters, 2007, 90, 052902.	3.3	62
167	Design strategies for MOF-derived porous functional materials: Preserving surfaces and nurturing pores. Journal of Materiomics, 2021, 7, 440-459.	5.7	62
168	Origin of a Tetragonal BiFeO ₃ Phase with a Giant <i>c</i> / <i>a</i> Ratio on SrTiO ₃ Substrates. Advanced Functional Materials, 2012, 22, 937-942.	14.9	61
169	Co/Zn bimetallic oxides derived from metal organic frameworks for high performance electrochemical energy storage. Electrochimica Acta, 2018, 291, 177-187.	5.2	60
170	Wafer-scale solution-processed 2D material analog resistive memory array for memory-based computing. Nature Communications, 2022, 13, .	12.8	60
171	Electrical behavior and oxygen vacancies in BiFeO3/[(Bi1/2Na1/2)0.94Ba0.06]TiO3 thin film. Applied Physics Letters, 2009, 95, .	3.3	59
172	Co-sensitization of TiO2 by PbS quantum dots and dye N719 in dye-sensitized solar cells. Thin Solid Films, 2010, 518, e54-e56.	1.8	59
173	Intercalating graphene with clusters of Fe ₃ O ₄ nanocrystals for electrochemical supercapacitors. Materials Research Express, 2014, 1, 025015.	1.6	59
174	Dynamic Surface Chemistry of Catalysts in Oxygen Evolution Reaction. Small Science, 2021, 1, 2100011.	9.9	59
175	Top-seeding melt texture growth of single-domain superconducting pellets. Superconductor Science and Technology, 1997, 10, 147-155.	3.5	58
176	Fine Strontium Ferrite Powders from an Ethanolâ€Based Microemulsion. Journal of the American Ceramic Society, 2000, 83, 1049-1055.	3.8	58
177	Labile Ferroelastic Nanodomains in Bilayered Ferroelectric Thin Films. Advanced Materials, 2009, 21, 3497-3502.	21.0	58
178	MOFâ€Derived Vertically Aligned Mesoporous Co ₃ O ₄ Nanowires for Ultrahigh Capacity Lithiumâ€Ion Batteries Anodes. Advanced Materials Interfaces, 2018, 5, 1800222.	3.7	58
179	Microstructural Origins of High Piezoelectric Performance: A Pathway to Practical Leadâ€Free Materials. Advanced Functional Materials, 2019, 29, 1902911.	14.9	58
180	Epsilon-negative BaTiO3/Cu composites with high thermal conductivity and yet low electrical conductivity. Journal of Materiomics, 2020, 6, 145-151.	5.7	58

#	Article	IF	CITATIONS
181	Nanosized Barium Titanate Powder by Mechanical Activation. Journal of the American Ceramic Society, 2000, 83, 232-34.	3.8	57
182	Ferroelectricity and ferroelectric resistive switching in sputtered Hf0.5Zr0.5O2 thin films. Applied Physics Letters, 2016, 108, .	3.3	57
183	Twinned Tungsten Carbonitride Nanocrystals Boost Hydrogen Evolution Activity and Stability. Small, 2019, 15, e1900248.	10.0	57
184	Electrospun Nanofibers for New Generation Flexible Energy Storage. Energy and Environmental Materials, 2021, 4, 502-521.	12.8	57
185	Rice husk-derived Mn ₃ O ₄ /manganese silicate/C nanostructured composites for high-performance hybrid supercapacitors. Inorganic Chemistry Frontiers, 2019, 6, 2788-2800.	6.0	56
186	Flexible and Wearable All-Solid-State Al–Air Battery Based on Iron Carbide Encapsulated in Electrospun Porous Carbon Nanofibers. ACS Applied Materials & Interfaces, 2019, 11, 1988-1995.	8.0	56
187	Ultrafine Barium Titanate Powders via Microemulsion Processing Routes. Journal of the American Ceramic Society, 1999, 82, 873-881.	3.8	55
188	Thickness and coupling effects in bilayered multiferroic CoFe2O4/Pb(Zr0.52Ti0.48)O3 thin films. Journal of Applied Physics, 2008, 103, .	2.5	55
189	Facile synthesis of hybrid silica nanocapsules by interfacial templating condensation and their application in fluorescence imaging. Chemical Communications, 2009, , 6240.	4.1	55
190	High-performance B4C–TiB2–SiC composites with tuneable properties fabricated by reactive hot pressing. Journal of the European Ceramic Society, 2019, 39, 2995-3002.	5.7	55
191	Synergizing aliovalent doping and interface in heterostructured NiV nitride@oxyhydroxide core-shell nanosheet arrays enables efficient oxygen evolution. Nano Energy, 2021, 85, 105961.	16.0	55
192	Swapping Catalytic Active Sites from Cationic Ni to Anionic S in Nickel Sulfide Enables More Efficient Alkaline Hydrogen Generation. Advanced Energy Materials, 2022, 12, .	19.5	55
193	Silica-shell cross-linked micelles encapsulating fluorescent conjugated polymers for targeted cellular imaging. Biomaterials, 2012, 33, 237-246.	11.4	54
194	Metal–Organic Frameworks (MOFs)-boosted filtration membrane technology for water sustainability. APL Materials, 2020, 8, .	5.1	54
195	Evolution from Leadâ€Based to Leadâ€Free Piezoelectrics: Engineering of Lattices, Domains, Boundaries, and Defects Leading to Giant Response. Advanced Materials, 2022, 34, e2106845.	21.0	54
196	Strong Charge Transfer at 2H–1T Phase Boundary of MoS ₂ for Superb Highâ€Performance Energy Storage. Small, 2019, 15, e1900131.	10.0	53
197	Recent advances and future perspectives for graphene oxide reinforced epoxy resins. Materials Today Communications, 2020, 23, 100883.	1.9	53
198	3D-printed surface-patterned ceramic membrane with enhanced performance in crossflow filtration. Journal of Membrane Science, 2020, 606, 118138.	8.2	53

JOHN WANG

#	Article	IF	CITATIONS
199	Microemulsion processing of manganese zinc ferrites. Materials Letters, 1997, 30, 217-221.	2.6	52
200	Supramolecular-Templated Thick Mesoporous Titania Films for Dye-Sensitized Solar Cells: Effect of Morphology on Performance. ACS Applied Materials & Interfaces, 2009, 1, 2789-2795.	8.0	52
201	Ferroelectric Behavior in Bismuth Ferrite Thin Films of Different Thickness. ACS Applied Materials & Interfaces, 2011, 3, 3261-3263.	8.0	52
202	(Ba, Ca)(Ti, Zr)O3-BiFeO3 lead-free piezoelectric ceramics. Current Applied Physics, 2012, 12, 534-538.	2.4	52
203	A novel hollowed CoO-in-CoSnO ₃ nanostructure with enhanced lithium storage capabilities. Nanoscale, 2014, 6, 13824-13830.	5.6	52
204	Heterogeneous ZIF-L membranes with improved hydrophilicity and anti-bacterial adhesion for potential application in water treatment. RSC Advances, 2019, 9, 1591-1601.	3.6	51
205	Robust pure copper framework by extrusion 3D printing for advanced lithium metal anodes. Journal of Materials Chemistry A, 2020, 8, 9058-9067.	10.3	51
206	Transparent magnetic composites of ZnFe2O4 nanoparticles in silica. Journal of Applied Physics, 2001, 90, 4169-4174.	2.5	50
207	Mesocrystals as a class of multifunctional materials. CrystEngComm, 2014, 16, 5948-5967.	2.6	50
208	Cu and Co nanoparticle-Co-decorated N-doped graphene nanosheets: a high efficiency bifunctional electrocatalyst for rechargeable Zn–air batteries. Journal of Materials Chemistry A, 2019, 7, 12851-12858.	10.3	50
209	Chemical-grafting of graphene oxide quantum dots (GOQDs) onto ceramic microfiltration membranes for enhanced water permeability and anti-organic fouling potential. Applied Surface Science, 2020, 502, 144128.	6.1	50
210	Nanocomposites of ZnFe2O4 in silica: synthesis, magnetic and optical properties. Materials Chemistry and Physics, 2002, 75, 181-185.	4.0	49
211	The effects of anodization parameters on titania nanotube arrays and dye sensitized solar cells. Nanotechnology, 2008, 19, 405701.	2.6	49
212	A Method to Improve Electrical Properties of BiFeO ₃ Thin Films. ACS Applied Materials & Interfaces, 2012, 4, 1182-1185.	8.0	49
213	Hydrothermal growth and optical properties of Nb ₂ O ₅ nanorod arrays. Journal of Materials Chemistry C, 2014, 2, 8185-8190.	5.5	49
214	Health Promotion Board–Ministry of Health Clinical Practice Guidelines: Obesity. Singapore Medical Journal, 2015, 57, 292-300.	0.6	49
215	Assembling of Bi atoms on TiO ₂ nanorods boosts photoelectrochemical water splitting of semiconductors. Nanoscale, 2020, 12, 4302-4308.	5.6	49
216	Developing better ceramic membranes for water and wastewater Treatment: Where microstructure integrates with chemistry and functionalities. Chemical Engineering Journal, 2022, 428, 130456.	12.7	49

#	Article	IF	CITATIONS
217	Highly efficient dyeâ€sensitized solar cells using phenothiazine derivative organic dyes. Progress in Photovoltaics: Research and Applications, 2010, 18, 573-581.	8.1	48
218	A new class of solid state ionic conductors for application in all solid state dye sensitized solar cells. Chemical Communications, 2010, 46, 2091.	4.1	48
219	Hypophosphite hybrid perovskites: a platform for unconventional tilts and shifts. Chemical Communications, 2018, 54, 3751-3754.	4.1	48
220	A sacrificial Zn strategy enables anchoring of metal single atoms on the exposed surface of holey 2D molybdenum carbide nanosheets for efficient electrocatalysis. Journal of Materials Chemistry A, 2020, 8, 3071-3082.	10.3	48
221	Improved ferroelectric behavior in (110) oriented BiFeO3 thin films. Journal of Applied Physics, 2010, 107, 034103.	2.5	47
222	All-solid-state sponge-like squeezable zinc-air battery. Energy Storage Materials, 2019, 23, 375-382.	18.0	47
223	Quasi-solid-state fiber-shaped aqueous energy storage devices: recent advances and prospects. Journal of Materials Chemistry A, 2020, 8, 6406-6433.	10.3	47
224	Effects of SRO Buffer Layer on Multiferroic BiFeO ₃ Thin Films. Journal of the American Ceramic Society, 2008, 91, 3240-3244.	3.8	46
225	Diodelike and resistive hysteresis behavior of heterolayered BiFeO3/ZnO ferroelectric thin films. Journal of Applied Physics, 2010, 108, .	2.5	46
226	A giant polarization value of Zn and Mn co-modified bismuth ferrite thin films. Applied Physics Letters, 2013, 102, .	3.3	46
227	Cobalt monoxide-doped porous graphitic carbon microspheres for supercapacitor application. Scientific Reports, 2013, 3, 2925.	3.3	46
228	Quench-tailored Al-doped V2O5 nanomaterials for efficient aqueous zinc-ion batteries. Journal of Energy Chemistry, 2022, 70, 52-58.	12.9	46
229	Overoxidized Poly{pyrrole-co-[3-(pyrrol-1-yl)- propanesulfonate]}-coated Platinum Electrodes for Selective Detection of Catecholamine Neurotransmitters. Analyst, The, 1997, 122, 981-984.	3.5	45
230	Mechanochemically Synthesized Lead Magnesium Niobate. Journal of the American Ceramic Society, 1999, 82, 1358-1360.	3.8	45
231	Phase transitions and electrical behavior of lead-free (K0.50Na0.50)NbO3 thin film. Journal of Applied Physics, 2009, 106, .	2.5	45
232	Nanohollow Carbon for Rechargeable Batteries: Ongoing Progresses and Challenges. Nano-Micro Letters, 2020, 12, 183.	27.0	45
233	Mechanochemical synthesis of nanosized lead titanate powders from mixed oxides. Materials Letters, 1999, 39, 364-369.	2.6	44
234	Phase transition, ferroelectric behaviors and domain structures of (Na1/2Bi1/2)1â^'xTiPbxO3 thin films. Acta Materialia, 2006, 54, 1691-1698.	7.9	44

#	Article	IF	CITATIONS
235	Ferroelectricity emerging in strained (111)-textured ZrO2 thin films. Applied Physics Letters, 2016, 108, .	3.3	44
236	From Well-Defined Carbon-Rich Precursors to Monodisperse Carbon Particles with Hierarchic Structures. Advanced Materials, 2007, 19, 1849-1853.	21.0	43
237	Toughening mechanisms in duplex alumina-zirconia ceramics. Journal of Materials Science, 1988, 23, 804-808.	3.7	42
238	Highly dispersed gold nanoparticles assembled in mesoporous titania films of cubic configuration. Microporous and Mesoporous Materials, 2008, 110, 242-249.	4.4	42
239	ZnO as a buffer layer for growth of BiFeO3 thin films. Journal of Applied Physics, 2010, 108, .	2.5	42
240	Tuning the porous texture and specific surface area of nanoporous carbons for supercapacitor electrodes by adjusting the hydrothermal synthesis temperature. Journal of Materials Chemistry A, 2013, 1, 12962.	10.3	42
241	Microwave – assisted hydrothermal synthesis of nanocrystal β-Ni(OH) ₂ for supercapacitor applications. CrystEngComm, 2016, 18, 3256-3264.	2.6	42
242	Open hollow Co–Pt clusters embedded in carbon nanoflake arrays for highly efficient alkaline water splitting. Journal of Materials Chemistry A, 2018, 6, 20214-20223.	10.3	42
243	Electronic-reconstruction-enhanced hydrogen evolution catalysis in oxide polymorphs. Nature Communications, 2019, 10, 3149.	12.8	42
244	Effect of gradient profile in ceramic membranes on filtration characteristics: Implications for membrane development. Journal of Membrane Science, 2020, 595, 117576.	8.2	42
245	Flexible quasi-solid-state aqueous Zn-based batteries: rational electrode designs for high-performance and mechanical flexibility. Materials Today Energy, 2020, 18, 100523.	4.7	42
246	Fabrication of 3D-Printed Ceramic Structures for Portable Solar Desalination Devices. ACS Applied Materials & Interfaces, 2021, 13, 23220-23229.	8.0	42
247	Dramatic effect of a small amount of MgO addition on the sintering of Al2O3-5 vol% SiC nanocomposite. Materials Letters, 1998, 33, 273-277.	2.6	41
248	Raman and magnetization studies of barium ferrite powder prepared by water-in-oil microemulsion. Journal of Materials Research, 2000, 15, 483-487.	2.6	41
249	Hydrothermal Growth of Vertical ZnO Nanorods. Journal of the American Ceramic Society, 2009, 92, 1940-1945.	3.8	41
250	Near-infrared emission from Eu–Yb doped silicate glasses subjected to thermal reduction. Applied Physics Letters, 2011, 98, .	3.3	41
251	Structural and topological aspects of borophosphate glasses and their relation to physical properties. Journal of Chemical Physics, 2015, 142, 184503.	3.0	41
252	Relaxivity and toxicological properties of manganese oxide nanoparticles for MRI applications. RSC Advances, 2016, 6, 45462-45474.	3.6	41

#	Article	IF	CITATIONS
253	Efficient Water Splitting System Enabled by Multifunctional Platinumâ€Free Electrocatalysts. Advanced Functional Materials, 2021, 31, 2009853.	14.9	41
254	Designing Poly[(<i>R</i>)-3-hydroxybutyrate]-Based Polyurethane Block Copolymers for Electrospun Nanofiber Scaffolds with Improved Mechanical Properties and Enhanced Mineralization Capability. Journal of Physical Chemistry B, 2010, 114, 7489-7498.	2.6	40
255	Growth rate induced monoclinic to tetragonal phase transition in epitaxial BiFeO3 (001) thin films. Applied Physics Letters, 2011, 98, 102902.	3.3	40
256	Nanoparticle morphology and film-forming behavior of polyacrylate/ZnO nanocomposite. Composites Science and Technology, 2014, 98, 64-71.	7.8	40
257	Silica–F127 nanohybrid-encapsulated manganese oxide nanoparticles for optimized T ₁ magnetic resonance relaxivity. Nanoscale, 2014, 6, 293-299.	5.6	40
258	pHâ€Activatable MnOâ€Based Fluorescence and Magnetic Resonance Bimodal Nanoprobe for Cancer Imaging. Advanced Healthcare Materials, 2016, 5, 721-729.	7.6	40
259	Photosynthetic apparatus of Rhodobacter sphaeroides exhibits prolonged charge storage. Nature Communications, 2019, 10, 902.	12.8	40
260	A negative-feedback loop maintains optimal chemokine concentrations for directional cell migration. Nature Cell Biology, 2020, 22, 266-273.	10.3	40
261	Fabrication and microstructure-mechanical property relationships in Ce-TZPs. Journal of Materials Science, 1992, 27, 5348-5356.	3.7	39
262	A Bicontinuous Microemulsion Route to Zinc Oxide Powder. Ceramics International, 1998, 24, 205-209.	4.8	39
263	Heterolayered lead zirconate titanate thin films of giant polarization. Journal of Applied Physics, 2004, 96, 5706-5711.	2.5	39
264	Single atom catalysts: a surface heterocompound perspective. Nanoscale Horizons, 2020, 5, 757-764.	8.0	39
265	Leakage current and charge carriers in (Na0.5Bi0.5)TiO3thin film. Journal Physics D: Applied Physics, 2005, 38, 642-648.	2.8	38
266	Charged defects and their effects on electrical behavior in Bi1â^'xLaxFeO3 thin films. Journal of Applied Physics, 2009, 105, 016106.	2.5	38
267	Impedance spectroscopy of bilayered bismuth ferrite thin films. Journal of Applied Physics, 2011, 110, .	2.5	38
268	Stable Ferroelectric Perovskite Structure with Giant Axial Ratio and Polarization in Epitaxial BiFe _{0.6} Ga _{0.4} O ₃ Thin Films. ACS Applied Materials & Interfaces, 2015, 7, 2648-2653.	8.0	38
269	Low-loss and temperature-stable negative permittivity in La0.5Sr0.5MnO3 ceramics. Journal of the European Ceramic Society, 2020, 40, 1917-1921.	5.7	38
270	Quenchâ€Induced Surface Engineering Boosts Alkaline Freshwater and Seawater Oxygen Evolution Reaction of Porous NiCo ₂ O ₄ Nanowires. Small, 2022, 18, e2106187.	10.0	38

#	Article	IF	CITATIONS
271	Degradable Cross-Linked Collagen Fiber/MXene Composite Aerogels as a High-Performing Sensitive Pressure Sensor. ACS Sustainable Chemistry and Engineering, 2022, 10, 1408-1418.	6.7	38
272	The effects of notch width on the SENB toughness for oxide ceramics. Journal of the European Ceramic Society, 1992, 10, 21-31.	5.7	37
273	Mechanochemical fabrication of single phase PMN of perovskite structure. Solid State Ionics, 1999, 124, 271-279.	2.7	37
274	Mechanochemical Synthesis of 0.9 Pb(Mg1/3Nb2/3)O3-0.1 PbTiO3from Mixed Oxides. Advanced Materials, 1999, 11, 210-213.	21.0	37
275	Effect of high-energy mechanical activation on the microstructure and electrical properties of ZnO-based varistors. Solid State Ionics, 2000, 132, 107-117.	2.7	37
276	Twinning rotation and ferroelectric behavior of epitaxial BiFeO3 (001) thin film. Applied Physics Letters, 2010, 96, .	3.3	37
277	Enhanced photovoltaic effects and switchable conduction behavior in BiFe0.6Sc0.4O3 thin films. Acta Materialia, 2015, 88, 83-90.	7.9	37
278	Hydrogenated TiO2 membrane with photocatalytically enhanced anti-fouling for ultrafiltration of surface water. Applied Catalysis B: Environmental, 2020, 264, 118528.	20.2	37
279	How different is mechanical activation from thermal activation? A case study with PZN and PZN-based relaxors. Solid State Ionics, 2000, 127, 169-175.	2.7	36
280	In vitro bioactivity assessment of 70 (wt.)%SiO2–30 (wt.)%CaO bioactive glasses in simulated body fluid. Materials Letters, 2005, 59, 3267-3271.	2.6	36
281	Probing the Microporous Structure of Silica Shell Via Aggregationâ€Induced Emission in Au(I)â€Thiolate@SiO ₂ Nanoparticle. Small, 2016, 12, 6537-6541.	10.0	36
282	Hollow structure engineering of FeCo alloy nanoparticles electrospun in nitrogen-doped carbon enables high performance flexible all-solid-state zinc–air batteries. Sustainable Energy and Fuels, 2020, 4, 1747-1753.	4.9	36
283	Fabricating densified hydroxyapatite ceramics from a precipitated precursor. Materials Letters, 1999, 38, 208-213.	2.6	35
284	Ultrafine zinc oxide powders prepared by precipitation/mechanical milling. Journal of Materials Science, 2001, 36, 3273-3276.	3.7	35
285	Phosphorusâ€Based Electrocatalysts: Black Phosphorus, Metal Phosphides, and Phosphates. Advanced Materials Interfaces, 2020, 7, 2000676.	3.7	35
286	Manipulating Interfaces of Electrocatalysts Down to Atomic Scales: Fundamentals, Strategies, and Electrocatalytic Applications. Small Methods, 2021, 5, e2001010.	8.6	35
287	Reduced crystallization temperature in a microemulsion-derived zirconia precursor. Materials Letters, 1997, 30, 119-124.	2.6	34
288	Comparative study on phase development of lead titanate powders. Materials Letters, 2002, 52, 304-312.	2.6	34

#	Article	IF	CITATIONS
289	Origin of the enhanced polarization in La and Mg co-substituted BiFeO3 thin film during the fatigue process. Applied Physics Letters, 2012, 100, .	3.3	34
290	Overcoming the Limits of the Interfacial Dzyaloshinskii–Moriya Interaction by Antiferromagnetic Order in Multiferroic Heterostructures. Advanced Materials, 2020, 32, e1904415.	21.0	34
291	Ultrafine zirconia powders via microemulsion processing route. Scripta Materialia, 1997, 8, 499-505.	0.5	33
292	Mechanochemical Synthesis of Hydroxyapatite from Calcium Oxide and Brushite. Journal of the American Ceramic Society, 2001, 84, 465-67.	3.8	33
293	A Hybrid Silica Nanoreactor Framework for Encapsulation of Hollow Manganese Oxide Nanoparticles of Superior T ₁ Magnetic Resonance Relaxivity. Advanced Functional Materials, 2015, 25, 5269-5276.	14.9	33
294	3D hierarchical SnO ₂ @Ni(OH) ₂ core–shell nanowire arrays on carbon cloth for energy storage application. Journal of Materials Chemistry A, 2015, 3, 9538-9542.	10.3	33
295	Large-area multifunctional electro-chromic-chemical device made of W17O47 nanowires by Zn2+ ion intercalation. Nano Energy, 2021, 89, 106356.	16.0	33
296	Thickness-dependent twinning evolution and ferroelectric behavior of epitaxial <mml:math xmlns:mml="http://www.w3.org/1998/Math/MathML" display="inline"><mml:mrow><mml:msub><mml:mrow><mml:mtext>BiFeO</mml:mtext></mml:mrow><mml:m thin films. Physical Review B, 2010, 82, .</mml:m </mml:msub></mml:mrow></mml:math 	າກ>32/mm	ו::::::::::::::::::::::::::::::::::::
297	Synthesis of Pb(Mg _{1/3} Nb _{2/3})O ₃ in Excess Lead Oxide by Mechanical Activation. Journal of the American Ceramic Society, 2001, 84, 660-662.	3.8	31
298	Dielectric relaxation in SrBi2(V0.1Nb0.9)2O9 layered perovskite ceramics. Materials Chemistry and Physics, 2002, 75, 50-55.	4.0	31
299	Functional ceramics of nanocrystallinity by mechanical activation. Solid State Ionics, 2002, 151, 403-412.	2.7	31
300	Modulated charged defects and conduction behaviour in doped BiFeO ₃ thin films. Journal Physics D: Applied Physics, 2009, 42, 162001.	2.8	31
301	0.90(Na0.5Bi0.5TiO3)-0.06BaTiO3-0.04K0.5Na0.5NbO3 Ferroelectric Thin Films Derived from Chemical Solutions. Journal of the American Ceramic Society, 2011, 94, 1331-1335.	3.8	31
302	Growth of centimeter-sized [(CH ₃) ₂ NH ₂][Mn(HCOO) ₃] hybrid formate perovskite single crystals and Raman evidence of pressure-induced phase transitions. New Journal of Chemistry, 2017, 41, 151-159.	2.8	31
303	Free-Standing Black Phosphorus Thin Films for Flexible Quasi-Solid-State Micro-Supercapacitors with High Volumetric Power and Energy Density. ACS Applied Materials & Interfaces, 2019, 11, 5938-5946.	8.0	31
304	Mechanicalâ€Activationâ€Triggered Gibbsiteâ€ŧoâ€Boehmite Transition and Activationâ€Derived Alumina Powders. Journal of the American Ceramic Society, 2001, 84, 1225-1230.	3.8	30
305	Bismuth Titanate from Mechanical Activation of a Chemically Coprecipitated Precursor. Journal of the American Ceramic Society, 2002, 85, 2660-2665.	3.8	30
306	Titania-PMMA nanohybrids of enhanced nanocrystallinity. Journal of Electroceramics, 2006, 16, 431-439.	2.0	30

#	Article	IF	CITATIONS
307	Ferroelectric and dielectric behavior of heterolayered PZT thin films. Journal of Applied Physics, 2007, 102, .	2.5	30
308	The effects of ethyl cellulose on PV performance of DSSC made of nanostructured ZnO pastes. Thin Solid Films, 2010, 518, e68-e71.	1.8	30
309	Ferroelastic domain wall dynamics in ferroelectric bilayers. Acta Materialia, 2010, 58, 5316-5325.	7.9	30
310	Bipolar and unipolar electrical fatigue in ferroelectric lead zirconate titanate thin films: An experimental comparison study. Journal of Applied Physics, 2010, 108, .	2.5	30
311	Doping cobalt hydroxide nanowires for better supercapacitor performance. Acta Materialia, 2015, 84, 20-28.	7.9	30
312	(K,Na)NbO ₃ Nanofiber-based Self-Powered Sensors for Accurate Detection of Dynamic Strain. ACS Applied Materials & Interfaces, 2015, 7, 4921-4927.	8.0	29
313	Confined Fe ₂ O ₃ Nanoparticles on Graphite Foam as Highâ€Rate and Stable Lithiumâ€Ion Battery Anode. Particle and Particle Systems Characterization, 2016, 33, 487-492.	2.3	29
314	Facile Synthesis of Chitosan-Coated Silica Nanocapsules via Interfacial Condensation Approach for Sustained Release of Vanillin. Industrial & Engineering Chemistry Research, 2018, 57, 6171-6179.	3.7	29
315	Progress and prospects of aberration-corrected STEM for functional materials. Ultramicroscopy, 2018, 194, 182-192.	1.9	29
316	Activating inverse spinel NiCo2O4 embedded in N-doped carbon nanofibers via Fe substitution for bifunctional oxygen electrocatalysis. Materials Today Physics, 2021, 17, 100353.	6.0	29
317	Quasiâ€Paired Pt Atomic Sites on Mo ₂ C Promoting Selective Fourâ€Electron Oxygen Reduction. Advanced Science, 2021, 8, e2101344.	11.2	29
318	Sequential Combination of Constituent Oxides in the Synthesis of Pb(Fe _{1/2} Nb _{1/2})O ₃ by Mechanical Activation. Journal of the American Ceramic Society, 2002, 85, 565-572.	3.8	28
319	Ferroelectric behaviors and charge carriers in Nd-doped Bi4Ti3O12 thin films. Journal of Applied Physics, 2005, 97, 034101.	2.5	28
320	(1Ââ^'Â <i>x</i>) <scp><scp>Ba</scp></scp> (<scp>Zr</scp> _{0.2} <scp>Ti</scp> _{0.8} Ferroelectric Thin Films Prepared from Chemical Solutions. Journal of the American Ceramic Society, 2012, 95, 986-991.) <s 3.8</s 	cp> <scp>O 28</scp>
321	Silica Nanocapsules of Fluorescent Conjugated Polymers and Superparamagnetic Nanocrystals for Dualâ€Mode Cellular Imaging. Chemistry - A European Journal, 2011, 17, 6696-6706.	3.3	28
322	Valence-driven electrical behavior of manganese-modified bismuth ferrite thin films. Journal of Applied Physics, 2011, 109, 124118.	2.5	28
323	In-situ surface self-reconstruction in ternary transition metal dichalcogenide nanorod arrays enables efficient electrocatalytic oxygen evolution. Journal of Energy Chemistry, 2021, 55, 10-16.	12.9	28
324	Single metal atoms catalysts—Promising candidates for next generation energy storage and conversion devices. EcoMat, 2022, 4, .	11.9	28

#	Article	IF	CITATIONS
325	Zincophilic 3D ZnOHF nanowire arrays with ordered and continuous Zn2+ Ion modulation layer enable long-term stable Zn metal anodes. Energy Storage Materials, 2022, 50, 435-443.	18.0	28
326	Surface toughening of TZP ceramics by low temperature ageing. Ceramics International, 1989, 15, 15-21.	4.8	27
327	Preparation and characterisation of ultrafine lead titanate (PbTiO3) powders. Journal of Materials Science, 1999, 34, 1943-1952.	3.7	27
328	Uniaxial strain-induced ferroelectric phase with a giant axial ratio in a (110) BiFeO <mml:math xmlns:mml="http://www.w3.org/1998/Math/MathML" display="inline"><mml:msub><mml:mrow /><mml:mn>3</mml:mn></mml:mrow </mml:msub>thin film. Physical Review B, 2013, 87, .</mml:math 	3.2	27
329	Structural Instability of Epitaxial (001) BiFeO3 Thin Films under Tensile Strain. Scientific Reports, 2014, 4, 4631.	3.3	27
330	The Atomic Circus: Small Electron Beams Spotlight Advanced Materials Down to the Atomic Scale. Advanced Materials, 2018, 30, e1802402.	21.0	27
331	Interfacial diffusion assisted chemical deposition (ID-CD) for confined surface modification of alumina microfiltration membranes toward high-flux and anti-fouling. Separation and Purification Technology, 2020, 235, 116177.	7.9	27
332	The effects of mechanical activation in synthesizing ultrafine barium ferrite powders from co-precipitated precursors. Journal of Materials Chemistry, 2000, 10, 1745-1749.	6.7	26
333	Unipolar and bipolar fatigue in antiferroelectric lead zirconate thin films and evidences for switching-induced charge injection inducing fatigue. Applied Physics Letters, 2010, 96, .	3.3	26
334	Anosmin1 Shuttles Fgf to Facilitate Its Diffusion, Increase Its Local Concentration, and Induce Sensory Organs. Developmental Cell, 2018, 46, 751-766.e12.	7.0	26
335	Nanodiamond decorated graphene oxide and the reinforcement to epoxy. Composites Science and Technology, 2018, 165, 9-17.	7.8	26
336	Overcoming the Trade-off between Water Permeation and Mechanical Strength of Ceramic Membrane Supports by Interfacial Engineering. ACS Applied Materials & Interfaces, 2021, 13, 29199-29211.	8.0	26
337	Ceramic-Polymer Composite Membranes for Water and Wastewater Treatment: Bridging the Big Gap between Ceramics and Polymers. Molecules, 2021, 26, 3331.	3.8	26
338	<scp>Threeâ€dimensional</scp> knotting of <scp>W₁₇O₄₇</scp> @ <scp>PEDOT</scp> : <scp>PSS</scp> nanowires enables <scp>highâ€performance</scp> flexible cathode for dualâ€functional electrochromic and electrochemical device. InformaÄnÃ-MateriÃ;ly, 2022, 4, .	17.3	26
339	Femtosecond third-order optical nonlinearity of BiFeO3. Optics Express, 2009, 17, 10970.	3.4	25
340	MnOx nanosheets for improved electrochemical performances through bilayer nano-architecting. Journal of Power Sources, 2015, 286, 394-399.	7.8	25
341	Controllable structure transitions of Mn ₃ O ₄ nanomaterials and their effects on electrochemical properties. Nanoscale Horizons, 2017, 2, 326-332.	8.0	25
342	Enhancing water permeation through alumina membranes by changing from cylindrical to conical nanopores. Nanoscale, 2019, 11, 9869-9878.	5.6	25

#	Article	IF	CITATIONS
343	Unlocking the synergy of interface and oxygen vacancy by core-shell nickel phosphide@oxyhydroxide nanosheets arrays for accelerating alkaline oxygen evolution kinetics. Chemical Engineering Journal, 2021, 425, 131491.	12.7	25
344	Direct ink writing of programmable functional siliconeâ€based composites for 4D printing applications. , 2022, 1, 507-516.		25
345	Zirconia toughened cordierite. Journal of Materials Science, 1990, 25, 3982-3989.	3.7	24
346	Synthesis of lead zirconate titanate from an amorphous precursor by mechanical activation. Journal of Alloys and Compounds, 2000, 308, 139-146.	5.5	24
347	Fabrication of YBa2Cu3O7â^'x (YBCO) superconductor bulk structures by extrusion freeforming. Ceramics International, 2016, 42, 15836-15842.	4.8	24
348	MOF-derived manganese oxide/carbon nanocomposites with raised capacitance for stable asymmetric supercapacitor. RSC Advances, 2020, 10, 34403-34412.	3.6	24
349	High temperature piezoelectric strontium bismuth titanate from mechanical activation of mixed oxides. Materials Chemistry and Physics, 2002, 75, 131-135.	4.0	23
350	Layer structured calcium bismuth titanate by mechanical activation. Materials Letters, 2004, 58, 2032-2036.	2.6	23
351	Fatigue and ferroelectric behavior of La and Zn comodified BiFeO3 thin films. Journal of Applied Physics, 2010, 108, .	2.5	23
352	Effect of manganese doping on the size effect of lead zirconate titanate thin films and the extrinsic nature of †dead layers'. Journal of Physics Condensed Matter, 2010, 22, 055901.	1.8	23
353	Formation and Anisotropic Dissolution Behavior of NH ₄ TiOF ₃ Mesocrystals. Crystal Growth and Design, 2011, 11, 2905-2912.	3.0	23
354	Manipulating the Formation of NH ₄ TiOF ₃ Mesocrystals: Effects of Temperature, Surfactant, and pH. Crystal Growth and Design, 2012, 12, 2625-2633.	3.0	23
355	Synthesis of Au-SiO ₂ Asymmetric Clusters and Their Application in ZnO Nanosheet-Based Dye-Sensitized Solar Cells. ACS Applied Materials & Interfaces, 2013, 5, 5601-5608.	8.0	23
356	Controlled growth of a metal–organic framework on gold nanoparticles. CrystEngComm, 2016, 18, 5262-5266.	2.6	23
357	Synthesis and Characterization of Silicaâ^'Copper Oxide Composite Derived from Microemulsion Processing. Langmuir, 1999, 15, 3056-3061.	3.5	22
358	Gene delivery to the heart by magnetic nanobeads. Journal of Magnetism and Magnetic Materials, 2007, 311, 336-341.	2.3	22
359	Tunable photoluminescence induced by thermal reduction in rare earth doped glasses. Journal of Materials Chemistry, 2011, 21, 6614.	6.7	22
360	<scp><scp>ZnO</scp></scp> Nanosheets Derived from Surfactantâ€Directed Process: Growth Mechanism, and Application in Dyeâ€Sensitized Solar Cells. Journal of the American Ceramic Society, 2012, 95, 1241-1246.	3.8	22

#	Article	IF	CITATIONS
361	An α–Fe ₂ O ₃ powder of nanosized particles via precursor dispersion. Journal of Materials Research, 1999, 14, 3355-3362.	2.6	21
362	B-site disordering in Pb(Sc1/2Ta1/2)O3 by mechanical activation. Applied Physics Letters, 2003, 82, 4773-4775.	3.3	21
363	Morphology, Optical, and Magnetic Properties of Zn _{1â^'<i>x</i>} Co _{<i>x</i>} O Nanorods Grown via a Wet Chemical Route. Journal of the American Ceramic Society, 2010, 93, 3798-3802.	3.8	21
364	Atomic-layer-deposition alumina induced carbon on porous Ni _x Co _{1 â^' x} O nanonets for enhanced pseudocapacitive and Li-ion storage performance. Nanotechnology, 2015, 26, 014001.	2.6	21
365	Hydrazine reduction of LaNiO ₃ for active materials in supercapacitors. Journal of the American Ceramic Society, 2017, 100, 4629-4637.	3.8	21
366	Room-temperature H2 gasochromic behavior of Pd-modified MoO3 nanowire labels. Materials Chemistry and Physics, 2019, 227, 111-116.	4.0	21
367	Lead zirconate titanate-barium titanate by mechanical activation of mixed oxides. Applied Physics A: Materials Science and Processing, 1999, 69, 433-436.	2.3	20
368	Significant dielectric enhancement in 0.3BiFeO3–0.7SrBi2Nb2O9. Applied Physics Letters, 2001, 79, 2061-2063.	3.3	20
369	Thickness dependences of ferroelectric and dielectric properties in (Bi3.15Nd0.85)Ti3O12 thin films. Journal of Applied Physics, 2006, 99, 074103.	2.5	20
370	Multiferroic BiFeO3Thin Films Buffered by a SrRuO3Layer. Journal of the American Ceramic Society, 2008, 91, 463-466.	3.8	20
371	Observation of a fifth-order optical nonlinearity in Bi0.9La0.1Fe0.98Mg0.02O3 ferroelectric thin films. Applied Physics Letters, 2009, 95, 041114.	3.3	20
372	Resistive hysteresis in BiFeO3 thin films. Materials Research Bulletin, 2011, 46, 2183-2186.	5.2	20
373	High optical performance and practicality of active plasmonic devices based on rhombohedral BiFeO ₃ . Laser and Photonics Reviews, 2012, 6, 684-689.	8.7	20
374	From NH ₄ TiOF ₃ nanoparticles to NH ₄ TiOF ₃ mesocrystals: steric hindrance versus hydrophobic attraction of F127 molecules. CrystEngComm, 2013, 15, 791-801.	2.6	20
375	Hollow Casein-Based Polymeric Nanospheres for Opaque Coatings. ACS Applied Materials & Interfaces, 2016, 8, 11739-11748.	8.0	20
376	NiFe Layered Double-Hydroxide Nanosheets on a Cactuslike (Ni,Co)Se ₂ Support for Water Oxidation. ACS Applied Nano Materials, 2019, 2, 325-333.	5.0	20
377	Surface engineered alumina microfiltration membranes based on rationally constructed core-shell particles. Journal of the European Ceramic Society, 2020, 40, 5951-5958.	5.7	20
378	Fiber-in-tube and particle-in-tube hierarchical nanostructures enable high energy density of MnO2-based asymmetric supercapacitors. Journal of Colloid and Interface Science, 2021, 582, 543-551.	9.4	20

#	Article	IF	CITATIONS
379	Effects of Chemical Species on the Crystallization Behavior of a Solâ€Derived Zirconia Precursor. Journal of the American Ceramic Society, 1998, 81, 2624-2628.	3.8	19
380	B-site ordering and magnetic behaviours in Ni-doped double perovskite Sr2FeMoO6. Journal Physics D: Applied Physics, 2005, 38, 4003-4008.	2.8	19
381	Ferroelectric and fatigue behavior of Pb(Zr0.52Ti0.48)O3â^•(Bi3.15Nd0.85)Ti3O12 bilayered thin films. Journal of Applied Physics, 2008, 103, 034102.	2.5	19
382	Resistive Hysteresis and Diodelike Behavior of BiFeO[sub 3]/ZnO Heterostructure. Electrochemical and Solid-State Letters, 2010, 13, G9.	2.2	19
383	Multiferroic behavior and electrical conduction of BiFeO3 thin film deposited on quartz substrate. Journal of Alloys and Compounds, 2010, 507, L4-L7.	5.5	19
384	Bendable graphene/conducting polymer hybrid films for freestanding electrodes with high volumetric capacitances. RSC Advances, 2016, 6, 2951-2957.	3.6	19
385	Mixed Xâ€6ite Formate–Hypophosphite Hybrid Perovskites. Chemistry - A European Journal, 2018, 24, 11309-11313.	3.3	19
386	Interfacial dielectric layer as an origin of polarization fatigue in ferroelectric capacitors. Scientific Reports, 2020, 10, 7310.	3.3	19
387	Alkali-deficiency driven charged out-of-phase boundaries for giant electromechanical response. Nature Communications, 2021, 12, 2841.	12.8	19
388	Formation and characterization of lead magnesium niobate synthesized from the molten salt of potassium chlorate. Journal of Alloys and Compounds, 1998, 274, 110-117.	5.5	18
389	Residual stress and magnetic behavior of multiferroic CoFe2O4/Pb(Zr0.52Ti0.48)O3 thin films. Journal of Applied Physics, 2009, 105, 084113.	2.5	18
390	Mn4+:BiFeO3/Zn2+:BiFeO3 bilayered thin films of (111) orientation. Applied Surface Science, 2011, 257, 7226-7230.	6.1	18
391	Polyacrylate/Surface-Modified ZnO Nanocomposite as Film-Forming Agent for Leather Finishing. International Journal of Polymeric Materials and Polymeric Biomaterials, 2014, 63, 809-814.	3.4	18
392	Microstructural evolution of charged defects in the fatigue process of polycrystalline BiFeO3 thin films. Acta Materialia, 2015, 82, 190-197.	7.9	18
393	Synthesis and characterization of ultrafine lead zirconate powders. Ceramics International, 1998, 24, 507-513.	4.8	17
394	Processing and Characterization of Microemulsionâ€Derived Lead Magnesium Niobate. Journal of the American Ceramic Society, 1999, 82, 529-536.	3.8	17
395	Improved Ferroelectric and Fatigue Behavior of Bi _{0.95} Gd _{0.05} FeO ₃ /BiFe _{0.95} Mn _{0.05} O _{3 Bilayered Thin Films. Journal of Physical Chemistry C, 2010, 114, 19318-19321.}		17
396	Multiferroic and fatigue behavior of silicon-based bismuth ferrite sandwiched structure. Journal of Materials Chemistry, 2011, 21, 7308.	6.7	17

#	Article	IF	CITATIONS
397	Fundamentals, On-Going Advances and Challenges of Electrochemical Carbon Dioxide Reduction. Electrochemical Energy Reviews, 2022, 5, 82-111.	25.5	17
398	Low temperature synthesis of PZT powders via microemulsion processing. Materials Research Bulletin, 1998, 33, 1045-1055.	5.2	16
399	Synthesis of nanocrystalline γ-Fe2O3 in silica matrix by mechanical crystallization from precursor at room temperature. Materials Chemistry and Physics, 2002, 75, 81-85.	4.0	16
400	Mechanical Activationâ€Assisted Synthesis of Pb(Fe _{2/3} W _{1/3})O ₃ . Journal of the American Ceramic Society, 2000, 83, 1575-1580.	3.8	16
401	BiFeO ₃ Thin Films Deposited on LaNiO ₃ â€Buffered SiO ₂ /Si Substrate. Journal of the American Ceramic Society, 2010, 93, 1422-1426.	3.8	16
402	A metastable cubic phase of sodium niobate nanoparticles stabilized by chemically bonded solvent molecules. Physical Chemistry Chemical Physics, 2016, 18, 33171-33179.	2.8	16
403	Phospho-oxynitride Layer Protected Cobalt Phosphonitride Nanowire Arrays for High-Rate and Stable Supercapacitors. ACS Applied Energy Materials, 2019, 2, 616-626.	5.1	16
404	Squaraine organic crystals with strong dipole effect toward stable lithium-organic batteries. Energy Storage Materials, 2021, 41, 240-247.	18.0	16
405	Solar-Driven Gas-Phase Moisture to Hydrogen with Zero Bias. ACS Nano, 2021, 15, 19119-19127.	14.6	16
406	One-step synthesis of nitrogen-doped carbon quantum dots for paper-based electrochemiluminescence detection of Cu2+ ions. Microchemical Journal, 2022, 174, 107057.	4.5	16
407	A study of the reaction of Y1Ba2Cu3O7-? superconducting ceramics with water. Journal of Materials Science, 1988, 23, 3393-3397.	3.7	15
408	Synthesis of single phase 0.9Pb[(Zn0.6Mg0.4)1/3Nb2/3O3]–0.1PbTiO3 by mechanically activating mixed oxides. Acta Materialia, 1999, 47, 2283-2291.	7.9	15
409	Ferroelectric properties and leakage current characteristics of radio-frequency-sputtered SrBi2(V0.1Nb0.9)2O9 thin films. Journal of Applied Physics, 2004, 96, 2181-2185.	2.5	15
410	0.67Pb(Mg1/3Nb2/3)O3–0.33PbTiO3 thin films derived from RF magnetron sputtering. Ceramics International, 2004, 30, 1539-1542.	4.8	15
411	Fatigue behavior of heterostructured Pb(Zr,Ti)O3â^•(Bi,Nd)4Ti3O12 ferroelectric thin films. Applied Physics Letters, 2006, 89, 122905.	3.3	15
412	Hybrid Titania Microspheres of Novel Superstructures Templated by Block Copolymers. Chemistry of Materials, 2011, 23, 2745-2752.	6.7	15
413	Highly (111)-Orientated BiFeO ₃ Thin Film Deposited on La _{0.67} Sr _{0.33} MnO ₃ Buffered Pt/TiO ₂ /SiO ₂ /Si (100) Substrate. Journal of the Electrochemical Society, 2011, 159. G11-G14.	2.9	15
414	Guided Assembly of Microporous/Mesoporous Manganese Phosphates by Bifunctional Organophosphonic Acid Etching and Templating. Advanced Materials, 2019, 31, e1901124.	21.0	15

#	Article	IF	CITATIONS
415	Polymorphism in M(H ₂ PO ₂) ₃ (M = V, Al, Ga) compounds with the perovskite-related ReO ₃ structure. Chemical Communications, 2019, 55, 2964-2967.	4.1	15
416	Combinational Design of Electronic Structure and Nanoarray Architecture Achieves a Lowâ€Overpotential Oxygen Electrode for Aprotic Lithium–Oxygen Batteries. Small Methods, 2020, 4, 1900619.	8.6	15
417	Ultrahigh piezoelectric coefficients of Li-doped (K,Na)NbO3 nanorod arrays with manipulated O-T phase boundary: Towards energy harvesting and self-powered human movement monitoring. Nano Energy, 2021, 86, 106072.	16.0	15
418	Preferred ZrO2(t) → ZrO2(m) transformation on the aged surface of TZP ceramics. Journal of Materials Science Letters, 1989, 8, 1195-1198.	0.5	14
419	Ion-Containing Membranes from Microemulsion Polymerization. Langmuir, 1999, 15, 3202-3205.	3.5	14
420	Mechanical activation synthesis and dielectric properties of 0.48PFN–0.36PFW–0.16PZN from mixed oxides. Journal of Alloys and Compounds, 2000, 311, 181-187.	5.5	14
421	Effects of mechanical activation on the formation of PbTiO3 from amorphous Pb–Ti–O precursor. Journal of Applied Physics, 2003, 93, 3470-3474.	2.5	14
422	Dielectric behaviors of Pb1â^'3x/2LaxTiO3 derived from mechanical activation. Journal of Applied Physics, 2004, 95, 4981-4988.	2.5	14
423	B‣ite Order–Disorder Transition in Pb(Mg _{1/3} Nb _{2/3})O ₃ –Pb(Mg _{1/2} W _{1/2})O _{ Triggered by Mechanical Activation. Journal of the American Ceramic Society, 2002, 85, 833-838.}	>33 ./s ub>	14
424	Inducing Crystallization in an Amorphous Lead Zirconate Titanate Precursor by Mechanical Activation. Journal of the American Ceramic Society, 1999, 82, 1641-1643.	3.8	14
425	Temperature-dependent electrical behavior of La0.7Sr0.3MnO3-buffered Bi0.9La0.1FeO3 thin films. Journal of Applied Physics, 2009, 106, .	2.5	14
426	Highly efficient dye-sensitized solar cells of thick mesoporous titania films derived from supramolecular templating. Nanotechnology, 2009, 20, 505602.	2.6	14
427	Large ZnO Mesocrystals of Hexagonal Columnar Morphology Derived from Liquid Crystal Templates. Journal of the American Ceramic Society, 2011, 94, 3267-3275.	3.8	14
428	Mechanochemical Synthesis of 0.9[0.6Pb(Zn _{1/3} Nb _{2/3})O ₃ ·0.4Pb(Mg _{1/3} Nb _{2/3} Journal of the American Ceramic Society, 2000, 83, 53-59.	>) &s sub>3	3⊲/ s ub>]Â∙0.
429	Nanocrystalline PbTiO3 powders from an amorphous Pb–Ti–O precursor by mechanical activation. Materials Chemistry and Physics, 2002, 75, 216-219.	4.0	13
430	Nanocrystalline Maghemite (γâ€Fe ₂ O ₃) in Silica by Mechanical Activation of Precursors. Journal of the American Ceramic Society, 2002, 85, 807-811.	3.8	13
431	Multiferroic behaviour and orientation dependence of lead-free (1) Tj ETQq1 1 0.784314 rgBT /Overlock 10 Tf 50 films. Journal Physics D: Applied Physics, 2009, 42, 195405.	107 Td (â´ 2.8	^' <i>x</i>)Bil 13
432	Oxygen-vacancy-mediated negative differential resistance in La and Mg co-substituted BiFeO3 thin film. Journal of Applied Physics, 2011, 110, 124102.	2.5	13

JOHN WANG

#	Article	IF	CITATIONS
433	Extrusion printing of a designed three-dimensional YBa ₂ Cu ₃ O _{7â^'x} superconductor with milled precursor powder. Journal of Materials Chemistry C, 2017, 5, 3382-3389.	5.5	13
434	Nanowires versus nanosheets – Effects of NiCo2O4 nanostructures on ceramic membrane permeability and fouling potential. Separation and Purification Technology, 2019, 215, 644-651.	7.9	13
435	Atomic-Scale Control of Magnetism at the Titanite-Manganite Interfaces. Nano Letters, 2019, 19, 3057-3065.	9.1	13
436	Electrochemiluminescence Detection of Sunset Yellow by Graphene Quantum Dots. Frontiers in Chemistry, 2020, 8, 505.	3.6	13
437	Direct Pyrolysis of a Manganeseâ€Triazolate Metal–Organic Framework into Airâ€Stable Manganese Nitride Nanoparticles. Advanced Science, 2021, 8, 2003212.	11.2	13
438	Aggregation-Induced Luminescence Based UiO-66: Highly Selective Fast-Response Styrene Detection. ACS Applied Materials & Interfaces, 2022, 14, 22510-22520.	8.0	13
439	Synthesis of lead zirconate powders via a polyaniline-mediated microemulsion processing route. Materials Letters, 1998, 36, 179-185.	2.6	12
440	Nanocrystalline Si3N4 with Si–C–N shell structure. Materials Letters, 2001, 49, 318-323.	2.6	12
441	Mechanical activation-induced sequential combination, morphotric segregation and order–disorder transformation in Pb-based relaxors. Materials Science and Engineering B: Solid-State Materials for Advanced Technology, 2003, 99, 63-69.	3.5	12
442	Effects of Excess Bi2O3 on the Ferroelectric Behavior of Nd-Doped Bi4Ti3O12 Thin Films. Journal of the American Ceramic Society, 2005, 88, 1037-1040.	3.8	12
443	A theoretical study of permeability enhancement for ultrafiltration ceramic membranes with conical pores and slippage. Physics of Fluids, 2019, 31, .	4.0	12
444	Phase stability and dielectric properties of (1â^'x)PFW+xPZN derived from mechanical activation. Solid State Ionics, 2000, 127, 285-293.	2.7	11
445	Structure characterization of BiFeO3–SrBi2Nb2O9 ceramics by mechanical activation. Materials Science and Engineering B: Solid-State Materials for Advanced Technology, 2003, 99, 116-120.	3.5	11
446	Multiferroic and Fatigue Behavior of (Bi[sub 0.90]La[sub 0.10])FeO[sub 3]/CoFe[sub 2]O[sub 4]/(Bi[sub) Tj ETQq G61.	0 0 0 rgBT 2.2	7 /Overlock 11
447	BiFeO3/Zn1â [~] 'xMnxO bilayered thin films. Applied Surface Science, 2011, 258, 1390-1394.	6.1	11
448	Combined effects of bilayer structure and ion substitutions on bismuth ferrite thin films. Journal of Applied Physics, 2011, 109, .	2.5	11
449	Ultraviolet photovoltaic effect in BiFeO3/Nb-SrTiO3 heterostructure. Journal of Applied Physics, 2012, 112, .	2.5	11
450	Negative capacitance induced by redistribution of oxygen vacancies in the fatigued BiFeO3-based thin film. Applied Physics Letters, 2012, 101, 022904.	3.3	11

#	Article	IF	CITATIONS
451	Nickel and Lanthanum Hydroxide Nanocomposites with Much Improved Electrochemical Performance for Supercapacitors. Journal of the American Ceramic Society, 2017, 100, 247-256.	3.8	11
452	Highly permeable Al 2 O 3 microfiltration membranes with holey interior structure achieved through sacrificial C particles. Journal of the American Ceramic Society, 2020, 103, 3361-3372.	3.8	11
453	Ultrathin TiO2 microfiltration membranes supported on a holey intermediate layer to raise filtration performance. Journal of the European Ceramic Society, 2021, 41, 1622-1628.	5.7	11
454	Recent progress in self-supported nanoarrays with diverse substrates for water splitting and beyond. Materials Today Nano, 2021, 15, 100120.	4.6	11
455	Origin of giant electric-field-induced strain in faulted alkali niobate films. Nature Communications, 2022, 13, .	12.8	11
456	Thermal stability of Al2O3-5 vol% SiC nanocomposite. Journal of Materials Science, 1995, 30, 321-333.	3.7	10
457	Synthesis and dielectric characterisation of lead magnesium niobate from precipitation and freeze-drying methods. Journal of Materials Chemistry, 1998, 8, 2239-2244.	6.7	10
458	A sol-gel derived 0.9Pb(Mg _{1/2} Nb _{2/3})O ₃ –0.1PbTiO ₃ ceramic. Journal of Materials Research, 1999, 14, 537-545.	2.6	10
459	Evidence of lower valence state of vanadium on the dielectric relaxation of ferroelectric SrBi2(V0.1Nb0.9)2O9. Journal Physics D: Applied Physics, 2002, 35, 2254-2259.	2.8	10
460	Nanosized Zincâ€Oxide Particles Derived from Mechanical Activation of Zn ₅ (NO ₃) ₂ (OH) ₈ ·2H ₂ O in Sodium Chloride. Journal of the American Ceramic Society, 2002, 85, 273-275.	3.8	10
461	Ferroelectric properties of heterolayered lead zirconate titanate thin films. Journal of Electroceramics, 2006, 16, 425-430.	2.0	10
462	Effect of <scp>(Bi,Gd)FeO₃</scp> Layer Thickness on the Microstructure and Electrical Properties of <scp>BiFeO₃</scp> Thin Films. Journal of the American Ceramic Society, 2011, 94, 4291-4298.	3.8	10
463	Sonochemical synthesis and liquid crystal assembly of PS-b-PEO–titania aggregates. Chemical Communications, 2012, 48, 8538.	4.1	10
464	Charge defects-induced electrical properties in bismuth ferrite bilayered thin films. Materials Research Bulletin, 2013, 48, 2973-2977.	5.2	10
465	Encapsulating Oxygenâ€Ðeficient TiNb ₂₄ O ₆₂ Microspheres by Nâ€Đoped Carbon Nanolayer Boosts Capacity and Stability of Lithiumâ€ŀon Battery. Batteries and Supercaps, 2020, 3, 1360-1369.	4.7	10
466	Hierarchically porous interlayer for highly permeable and fouling-resistant ceramic membranes in water treatment. Separation and Purification Technology, 2022, 293, 121092.	7.9	10
467	Modification of indentation cracks in TZP ceramics by thermal treatment. Journal of Materials Science Letters, 1988, 7, 560-562.	0.5	9
468	The effects of hydroxide gel drying on the characteristics of co-precipitated zirconia-hafnia powders. Journal of Materials Science, 1993, 28, 553-560.	3.7	9

#	Article	IF	CITATIONS
469	Crystallization in nanosized sol-derived zirconia precursors. Journal of Materials Science Letters, 1996, 15, 1680-1683.	0.5	9
470	Ferroelectric lead scandium tantalate from mechanical activation of mixed oxides. Materials Chemistry and Physics, 2002, 75, 157-160.	4.0	9
471	TRANSPARENT TIO2-PMMA NANOHYBRIDS OF HIGH NANOCRYSTALLINITY AND ENHANCED NONLINEAR OPTICAL PROPERTIES. Journal of Nonlinear Optical Physics and Materials, 2005, 14, 281-297.	1.8	9
472	Heterolayered PZT thin films of different thicknesses and stacking sequence. Journal of Materials Science, 2009, 44, 5375-5382.	3.7	9
473	Microstructure and texture development in single layered and heterolayered PZT thin films. Journal of Materials Science, 2010, 45, 6187-6199.	3.7	9
474	Multiferroic Behavior of Sn-Modified BiFeO[sub 3] Thin Films. Electrochemical and Solid-State Letters, 2010, 13, G83.	2.2	9
475	Effect of bilayer structure and a SrRuO3 buffer layer on ferroelectric properties of BiFeO3 thin films. Applied Physics A: Materials Science and Processing, 2012, 109, 57-61.	2.3	9
476	PEO surface-decorated silica nanocapsules and their application in in vivo imaging of zebrafish. RSC Advances, 2012, 2, 12392.	3.6	9
477	Tunneling electroresistance effect in ultrathin BiFeO3-based ferroelectric tunneling junctions. Applied Physics Letters, 2016, 109, .	3.3	9
478	Alumina double-layered ultrafiltration membranes with enhanced water flux. Colloids and Surfaces A: Physicochemical and Engineering Aspects, 2020, 587, 124324.	4.7	9
479	MnO2 as an effective sintering aid for difficult-to-sinter LiTaO3-based ceramics: Densification and dielectric properties. Journal of Alloys and Compounds, 2020, 829, 154546.	5.5	9
480	"Porous and Yet Dense―Electrodes for Highâ€Volumetricâ€Performance Electrochemical Capacitors: Principles, Advances, and Challenges. Advanced Science, 2022, 9, e2103953.	11.2	9
481	The microstructure of pressureless sintered silver-toughened alumina: an in situ TEM study. Materials Science & Engineering A: Structural Materials: Properties, Microstructure and Processing, 1993, 161, 119-126.	5.6	8
482	The grain boundary modification of ceria-stabilized tetragonal zirconia polycrystals by a small amount of alumina addition. Journal of Materials Science Letters, 1993, 12, 702-705.	0.5	8
483	Crystallization in seeded zirconia precipitates. Materials Letters, 1996, 27, 239-246.	2.6	8
484	Synthesizing 0.9PZN–0.1BT by mechanically activating mixed oxides. Solid State Ionics, 1999, 120, 183-188.	2.7	8
485	Cluster glass structure in nanohybrids of nonstoichiometric zinc ferrite in silica matrix. Applied Physics Letters, 2001, 79, 3167-3169.	3.3	8
486	Pb(Fe2/3W1/3)O3 by mechanical activation of coprecipitated Pb3Fe2O6 and WO3. Journal of Alloys and Compounds, 2002, 343, 156-163.	5.5	8

#	Article	IF	CITATIONS
487	Ferroelectric Pb(Mg1/3Nb2/3)O3 thin films by PLD at varying oxygen pressures. Microelectronic Engineering, 2003, 66, 926-932.	2.4	8
488	Polarization behaviors of (Bi3.15Nd0.85)Ti3O12 thin films deposited by radio-frequency magnetron sputtering. Journal of Applied Physics, 2005, 98, 104106.	2.5	8
489	Effect of Zn Concentration on Multiferroic and Fatigue Behavior of Bi[sub 0.90]La[sub 0.10]Fe[sub 1â°x]Zn[sub x]O[sub 3] Thin Films. Electrochemical and Solid-State Letters, 2010, 13, G105.	2.2	8
490	Unit-cell determination of epitaxial thin films based on reciprocal-space vectors by high-resolution X-ray diffractometry. Journal of Applied Crystallography, 2014, 47, 402-413.	4.5	8
491	Ferroelectric polarization relaxation in Au/Cu2O/ZnO/BiFeO3/Pt heterostructure. Applied Physics Letters, 2015, 106, .	3.3	8
492	Recent progress, developing strategies, theoretical insights, and perspectives towardsÂhigh-performance copper single atom electrocatalysts. Materials Today Energy, 2021, 21, 100761.	4.7	8
493	Stabilization of perovskite phase and dielectric properties of 0.95PZN–0.05BT derived from mechanical activation. Journal of Alloys and Compounds, 2000, 297, 92-98.	5.5	7
494	Structure and electrical properties of (100)-oriented Pb(Zn1/3Nb2/3)O3–Pb(Mg1/3Nb2/3)O3–PbTiO3 thin films on La0.7Sr0.3MnO3 electrode by chemical solution deposition. Thin Solid Films, 2008, 516, 5057-5061.	1.8	7
495	Formation and Evolution of Body entered Orthorhombic Mesophase in TiO ₂ Thin Films. Journal of the American Ceramic Society, 2009, 92, 1317-1321.	3.8	7
496	Evaporationâ€induced Alignment of Cylindrical Mesopores in TiO ₂ Thin Films. Journal of the American Ceramic Society, 2010, 93, 365-369.	3.8	7
497	Multiferroic behavior of BiFeO3–RTiO3 (Mg, Sr, Ca, Ba, and Pb) thin films. Journal of Applied Physics, 2010, 108, 026101.	2.5	7
498	Effect of oxygen content during sputtering on the electrical properties of bismuth ferrite thin films. Physica Status Solidi - Rapid Research Letters, 2011, 5, 190-192.	2.4	7
499	Membrane Fouling: Microscopic Insights into the Effects of Surface Chemistry and Roughness. Advanced Theory and Simulations, 0, , 2100395.	2.8	7
500	Two-step pyrolysis of Mn MIL-100 MOF into MnO nanoclusters/carbon and the effect of N-doping. Journal of Materials Chemistry A, 2022, 10, 8172-8177.	10.3	7
501	The loading rate dependence of fracture strength in a reaction-sintered mullite ceramic. Journal of Materials Science Letters, 1992, 11, 1201-1205.	0.5	6
502	Effects of organic binders on the sintering of isostatically compacted zirconia powders. Journal of Materials Science, 1992, 27, 63-67.	3.7	6
503	Lead Zirconate Titanate Via Reaction Sintering of Hydroxide Precursors. Journal of Materials Research, 1999, 14, 1503-1509.	2.6	6
504	Seeding effect in the formation of Pb(Fe2/3W1/3)O3 via mechanical activation of mixed oxides. Solid State lonics, 2000, 132, 55-61.	2.7	6

#	Article	IF	CITATIONS
505	Strontium–titanate-doped lead metaniobate ferroelectric thin films. Applied Physics Letters, 2002, 81, 877-879.	3.3	6
506	Ferroelectric and dielectric properties of 0.6SrBi2Nb2O9–0.4BiFeO3 thin films. Thin Solid Films, 2004, 460, 1-6.	1.8	6
507	Ferroelectric Bi4–x Sm x Ti3 O12 Thin Films Fabricated by Pulsed Laser Deposition for Nv-RAM Applications. Integrated Ferroelectrics, 2004, 61, 123-127.	0.7	6
508	Enhancement of Magnetization and Curie Temperature in Sr2FeMoO6 by Ni Doping. Journal of the American Ceramic Society, 2006, 89, 672-674.	3.8	6
509	Bilayered BiFe _{0.95} Mn _{0.05} O ₃ /Bi _{0.90} La _{0.10} FeO _{3Thin Films with Low Ferroelectric Coercivity and Large Remanent Polarization. Journal of the American Ceramic Society. 2010. 93. 2113-2116.}	sub> 3.8	6
510	Preparation and characterization of multiferroic CoFe2O4/Bi0.97Ce0.03FeO3 coaxial nanotubes. Applied Physics A: Materials Science and Processing, 2012, 108, 829-834.	2.3	6
511	Nanoscale phase mixture in uniaxial strained BiFeO3 (110) thin films. Journal of Applied Physics, 2015, 118, .	2.5	6
512	Revealing the hydrothermal crystallization mechanism of ilmenite-type sodium niobate microplates: the roles of potassium ions. CrystEngComm, 2017, 19, 5966-5972.	2.6	6
513	Water Permeation through Conical Nanopores: Complex Interplay between Surface Roughness and Chemistry. Advanced Theory and Simulations, 2020, 3, 2000025.	2.8	6
514	A quantitative X-ray diffraction phase analysis in the reaction-sintered mullite ceramics. Journal of Materials Science Letters, 1992, 11, 1301-1304.	0.5	5
515	Abnormal grain growth in alumina-doped hafnia ceramics. Journal of Materials Science, 1994, 29, 3577-3590.	3.7	5
516	Sintering and microstructural development of La0.80Ca0.22CrO3. Journal of Materials Science Letters, 1996, 15, 658-661.	0.5	5
517	Title is missing!. Catalysis Letters, 2000, 64, 179-184.	2.6	5
518	Doping effects of BiFeO3 in layered perovskite SrBi2Nb2O9. Materials Chemistry and Physics, 2002, 75, 105-109.	4.0	5
519	Mechanical activation-induced B site order–disorder transition in perovskite Pb(Mg1/3Nb2/3)O3–Pb(Mg1/2W1/2)O3. Materials Chemistry and Physics, 2002, 75, 211-215.	4.0	5
520	Mechanically Activated Synthesis and Magnetoresistance of Nanocrystalline Double Perovskite Sr2FeMoO6. Journal of the American Ceramic Society, 2005, 88, 2635-2638.	3.8	5
521	Mesophase configurations and optical properties of mesoporous TiO2 thin films. Journal of Electroceramics, 2006, 16, 499-502.	2.0	5
522	Ferroelectric and conductivity behavior of multilayered PbZr0.52Ti0.48O3â^•Pb(Mg1â^•3Ta2â^•3)0.7Ti0.3O3â^•PbZr0.52Ti0.48O3 thin films. Journal of Applied Physics, 20 100, 034106.)0265	5

#	Article	IF	CITATIONS
523	Peculiar Dielectric Behaviors of (Na1/2Bi1/2)0.87Pb0.13TiO3Thin Films. Journal of the American Ceramic Society, 2007, 90, 111-115.	3.8	5
524	Thickness-Dependent Magnetic Properties of Bismuth Ferrite Thin Films. Electrochemical and Solid-State Letters, 2011, 14, G57.	2.2	5
525	Kinetic study of solid phase crystallisation of expanding thermal plasma deposited a-Si:H. Thin Solid Films, 2012, 520, 5820-5825.	1.8	5
526	Dielectric dispersion and impedance spectroscopy of B3+-doped Ba(Ti0.9Sn0.1)O3 ceramics. Ceramics International, 2013, 39, S145-S148.	4.8	5
527	Ferroelectricity and dipole-dipole interactions in NH4TiOF3 mesocrystals. Applied Physics Letters, 2013, 102, 232903.	3.3	5
528	In situ electrochemical oxidation of electrodeposited Ni-based nanostructure promotes alkaline hydrogen production. Nanotechnology, 2019, 30, 474001.	2.6	5
529	Single Atom Electrocatalysis: Heterogeneous Single Atom Electrocatalysis, Where "Singles―Are "Married―(Adv. Energy Mater. 9/2020). Advanced Energy Materials, 2020, 10, 2070037.	19.5	5
530	Nanocrystalline 0.54PZN–0.36PMN–0.1PT of perovskite structure by mechanical activation. Materials Science & Engineering A: Structural Materials: Properties, Microstructure and Processing, 2000, 286, 96-100.	5.6	4
531	The B-site order-disorder transformation in Pb(Sc _{1/2} Ta _{1/2})O ₃ triggered by mechanical activation. Journal of Materials Science, 2004, 39, 5267-5270.	3.7	4
532	Ferroelectric properties and leakage current mechanisms in SrBi2(V0.1Nb0.9)2O9 (SBVN) thin films. Ceramics International, 2004, 30, 1505-1508.	4.8	4
533	Ferroelectric crossovers triggered by isovalent A-site substitution in Pb0.7La0.2TiO3. Journal of Applied Physics, 2006, 100, 124101.	2.5	4
534	Conducting perovskite LaNi0.6Co0.4O3 ceramics with glass additions. Journal of Electroceramics, 2006, 16, 313-319.	2.0	4
535	Structure and Optical Properties of 0.1BiFeO3-0.9SrBi2Nb2O9 Thin Films Using a Modified Sol-Gel Technique. Journal of Sol-Gel Science and Technology, 2006, 37, 27-30.	2.4	4
536	Pre-curing of supramolecular-templated mesoporous TiO2 films for dye-sensitized solar cells. Thin Solid Films, 2010, 518, e34-e37.	1.8	4
537	Compositionally graded bismuth ferrite thin films. Journal of Alloys and Compounds, 2011, 509, L319-L323.	5.5	4
538	Thin film bilayers of multiferroic bismuth ferrite on Pt–Si substrate. Physica Status Solidi - Rapid Research Letters, 2011, 5, 83-85.	2.4	4
539	Leakage behaviors of ferroelectric (Bi3.15Nd0.85)Ti3O12 thin film derived from RF sputtering. Applied Physics A: Materials Science and Processing, 2011, 105, 997-1001.	2.3	4
540	Multiferroic and fatigue behavior of BiFe _{0.95} Mn _{0.05} O ₃ /Bi _{0.90} La _{0.10} Fe _{0.8 bilayered thin films. IEEE Transactions on Ultrasonics, Ferroelectrics, and Frequency Control, 2012, 59, 14-20.}	5Zn	<syb>0.15</syb>

.

#	Article	IF	CITATIONS
541	Origin of dielectric anomaly in double perovskite Ba2CoNbO6. Ceramics International, 2014, 40, 14607-14612.	4.8	4
542	Exchange bias in tetragonal-like BiFeO 3 /Sr 2 FeMoO 6 bilayer. Journal of Magnetism and Magnetic Materials, 2018, 464, 156-160.	2.3	4
543	3D spray-coated gradient profile ceramic membranes enables improved filtration performance in aerobic submerged membrane bioreactor. Water Research, 2022, 220, 118661.	11.3	4
544	Mullitization in Al2O3-SiC nanocomposite: A case study of high temperature oxidation. Scripta Materialia, 1996, 34, 935-940.	5.2	3
545	A Monte Carlo simulation of B-site orderÂdisorder transformation in Pb(Sc1/2Ta1/2)O3triggered by mechanical activation. Journal of Physics Condensed Matter, 2002, 14, 8639-8653.	1.8	3
546	Effects of precursor solution pH value and substrate texture on orientation degree of sol–gel-derived bismuth titanate thin films. Physica Status Solidi A, 2003, 198, 282-288.	1.7	3
547	Ferroelectric Behaviors of W-Doped SrBi2Ta2O9 Thin Films. Integrated Ferroelectrics, 2004, 62, 163-169.	0.7	3
548	Dielectric behaviors and phase separation in Pb(Ni1/2W1/2)O3–PbTiO3. Ceramics International, 2004, 30, 1361-1364.	4.8	3
549	Phase Formation and Magnetoresistance of Double Perovskite Sr2FeMoO6. Journal of the American Ceramic Society, 2005, 88, 3279-3282.	3.8	3
550	The low-temperature synthesis of BiFeO3–SrBi2Nb2O9 complexes by sol-gel process. Materials Letters, 2005, 59, 912-915.	2.6	3
551	Effects of Ni doping on B-site ordering and magnetic behaviors of double perovskite Sr2FeMoO6. Journal of Electroceramics, 2006, 16, 351-355.	2.0	3
552	Ferroelectric properties of (Bi3.15 Nd 0.85)Ti 3 O 12 with decreasing film thickness. Journal of Electroceramics, 2006, 16, 477-481.	2.0	3
553	RF SPUTTERED BISMUTH FERRITE THIN FILMS: EFFECT OF ANNEALING DURATION. Functional Materials Letters, 2008, 01, 221-224.	1.2	3
554	Multiferroic, Optical, and Fatigue Behavior of BiFeO[sub 3] Thin Films with a Sintering Aid of CuO. Electrochemical and Solid-State Letters, 2010, 13, G68.	2.2	3
555	Freezeâ€dried graphene oxide modified with trimethylhexamethylene in the mix solvent for improved antiâ€corrosion property of epoxy. Journal of Applied Polymer Science, 2020, 137, 49139.	2.6	3
556	One-pot hydrothermal synthesis of fluorescent carbon quantum dots with tunable emission color for application in electroluminescence detection of dopamine. Biosensors and Bioelectronics: X, 2022, 10, 100141.	1.7	3
557	Melded ceramic membranes: A novel fabrication method for ultrathin alumina membranes of high performance. Journal of the American Ceramic Society, 2022, 105, 6554-6569.	3.8	3
558	An application of sol gelation in the dispersion mixing of ceramic-matrix composites. Journal of Materials Science Letters, 1992, 11, 807-809.	0.5	2

#	Article	IF	CITATIONS
559	Unique Dielectric Behavior of 0.6Pb(Ni _{1/2} W _{1/2})O ₃ ·0.4PbTiO ₃ Derived from Mechanical Activation. Journal of the American Ceramic Society, 2003, 86, 791-794.	3.8	2
560	Structural and Optical Properties of Lead Titanate Nanowires Synthesized by Hydrothermal Method. Key Engineering Materials, 2007, 336-338, 2157-2159.	0.4	2
561	Microcrack coalescence in alumina-zirconia composites. Journal of Materials Science Letters, 1996, 15, 442-444.	0.5	2
562	The closure of indentation cracks and strength recovery by low temperature ageing in Y-TZP. Scripta Metallurgica Et Materialia, 1992, 27, 815-820.	1.0	1
563	Crystallization of Lead Niobate Glass by Mechanical Activation. Journal of the American Ceramic Society, 2001, 84, 2691-2695.	3.8	1
564	Nanocrystalline ferroelectric phases from mechanical activation of oxide compositions. Scripta Materialia, 2001, 44, 1803-1806.	5.2	1
565	Ferroelectric and Dielectric Properties of Pb(Mg1/3Ta2/3)0.7Ti0.3O3 Thin Films Derived from RF Magnetron Sputtering. Journal of the American Ceramic Society, 2005, 88, 2769-2774.	3.8	1
566	Layer Structured Calcium Bismuth Titanate by Mechanical Activation. Journal of Metastable and Nanocrystalline Materials, 2005, 23, 47-50.	0.1	1
567	Ferroelectric and Dielectric Properties of Bilayered PMN–PT/BNdT Thin Films. Journal of the American Ceramic Society, 2006, 89, 2481-2485.	3.8	1
568	Dielectric anomalies of Pb0.7La0.2TiO3-based perovskite. Journal of Electroceramics, 2006, 16, 277-282.	2.0	1
569	Bilayered Pb(Zr,Ti)O3/(Bi,Nd)4Ti3O12 thin films. Journal of Electroceramics, 2006, 16, 459-462.	2.0	1
570	Ferroelectric transitions by Ca substitution in Pb0.7Nd0.2TiO3. Journal of Applied Physics, 2008, 103, 084114.	2.5	1
571	The Nanocrystallinity Enhancement of Sol-Gel Derived TiO ₂ Nanoparticles by Pre-Hydrothermal Treatment. Advanced Materials Research, 0, 415-417, 715-719.	0.3	1
572	Mesoporous Hollow Carbon Derived from Soft-Templated Hydrothermal Process for Supercapacitor Electrode. Key Engineering Materials, 0, 616, 134-140.	0.4	1
573	Composites, Nanocomposites and Hybrid Materials. , 2016, , 21-36.		1
574	Designing Energy Materials via Atomic-resolution Microscopy and Spectroscopy. Microscopy and Microanalysis, 2019, 25, 1998-1999.	0.4	1
575	Large-Scale Epitaxial Growth of Ultralong Stripe BiFeO3 Films and Anisotropic Optical Properties. ACS Applied Materials & Interfaces, 2022, , .	8.0	1
576	The effects of a small Al2O3 addition on the crystallization and densification of Na2O-stabilized silica sols. Journal of Materials Science Letters, 1992, 11, 1029-1032.	0.5	0

JOHN WANG

#	Article	IF	CITATIONS
577	Post-Sinter Annealing of Pb0.7La0.2TiO3 Derived from Mechanical Activation. Integrated Ferroelectrics, 2004, 62, 35-41.	0.7	0
578	Residual strains and dielectric properties of Pb/sub 0.7/La/sub 0.2/TiO/sub 3/-based perovskites. , 0, , .		0
579	Dieletric anomalies in Pb0.7(1â^'x)Ca0.7xLa0.2TiO3. Applied Physics Letters, 2005, 87, 072904.	3.3	0
580	Pb(Zn1/3Ta2/3)O3-PbTiO3 Derived from Mechanical Activation. Journal of the American Ceramic Society, 2006, 89, 060623005134009-???.	3.8	0
581	Ferroelectric behaviors of sandwich structured PbZr0.52 Ti0.48O3/Pb(Mg1/3Ta2/3)0.7Ti0.3O3/PbZr0.52Ti0.48O3 thin film. Journal of Electroceramics, 2006, 16, 453-457.	2.0	0
582	Heterolayered Ferroelectric Pb(Zr,Ti)O <inf>3</inf> /(Bi,Nd) <inf>4</inf> Ti <inf>3</inf> O <inf>12</inf> Thin Films. Applications of Ferroelectrics, IEEE International Symposium on, 2007, , .	0.0	0
583	Phase transition behaviors of (Na1/2Bi1/2)1â^'x TiPb x O3 thin films. Journal of Electroceramics, 2008, 21, 336-339.	2.0	0
584	Bilayered Pb(Zr,Ti)O3/(Bi,Nd)4Ti3O12 thin films. Journal of Electroceramics, 2008, 21, 331-335.	2.0	0
585	Bismuth ferrite bilayered thin films of different constituent layer thicknesses. Journal of Alloys and Compounds, 2011, 509, 7742-7748.	5.5	0
586	Effective control of polarity in Bi _{0.9} La _{0.1} FeO ₃ thin films by dopantâ€related internal bias. Physica Status Solidi (A) Applications and Materials Science, 2011, 208, 919-923.	1.8	0
587	Nanostructured Mesoporous Thick Films of Titania for Dye-Sensitized Solar Cells. Applied Mechanics and Materials, 0, 110-116, 540-546.	0.2	0
588	Optical Properties of 0.95BiFeO ₃ -RTiO ₃ (R = Mg, Pb, Ba, Ca and Sr) Thin Films. Integrated Ferroelectrics, 2012, 139, 1-6.	0.7	0
589	Solar Energy and Energy Storage Materials and Devices Research in Singapore. , 2016, , 113-156.		0